Summer 2024

Computational Fluid Dynamics Analysis of Thermal-Hydraulic Phenomena in Nuclear Reactor Systems

Mehedi Hasan Tusar
Missouri University of Science and Technology

Department:

COMPUTATIONAL FLUID DYNAMICS ANALYSIS OF THERMAL-HYDRAULIC PHENOMENA IN NUCLEAR REACTOR SYSTEMS

by

MEHEDI HASAN TUSAR

A THESIS

Presented to the Graduate Faculty of the

MISSOURI UNIVERSITY OF SCIENCE AND TECHNOLOGY

In Partial Fulfillment of the Requirements for the Degree

MASTER OF SCIENCE

in

NUCLEAR ENGINEERING

2024

Approved by:

Shoaib Usman, Advisor
Joseph Newkirk
Syed Alam

PUBLICATION DISSERTATION OPTION

This dissertation consists of the following two articles, formatted in the style used by the Missouri University of Science and Technology:

Paper I, found on pages 4-38, has been published in *International Communications in Heat and Mass Transfer*.

Paper II, found on pages 39–68, has been under review in *Experimental and Computational Multiphase Flow.*

ABSTRACT

A computational analysis of thermal-hydraulic processes in nuclear reactor systems is performed, leveraging Computational Fluid Dynamics (CFD) to advance the design and ensure the safety of nuclear reactors. Divided into two primary sections, the initial part examines thermal-hydraulic behavior in the Replacement Research Reactor (RRR) operating at 20 megawatts and evaluates potential enhancements for the Missouri University of Science and Technology Reactor (MSTR) to operate at an increased capacity of 2 megawatts from the existing 0.2 megawatts. Detailed simulations reveal insights into flow characteristics, temperature distributions, and pressure drops, highlighting the effective use of realistic and porous media modeling techniques for different reactor configurations. The second study investigates the complex flow dynamics of liquid-gas medium in sealed vessels across superhydrophilic to superhydrophobic wettability conditions. Employing CFD simulations alongside the VOF method with sharp interface accuracy, the study examines how factors such as contact angle, channel diameter, gravity, and viscosity influence flow patterns and blockages in closed environments. Results show that surface wettability and channel diameter significantly influence fluid behavior, with gravity variations further affecting flow dynamics in adiabatic, closed systems, offering insights for engineering design optimization. This comprehensive computational study explains the thermal-hydraulic processes in nuclear reactors and closed fluid systems, employing advanced CFD techniques to enhance design and safety.

ACKNOWLEDGEMENTS

I stand at the end of this academic journey with a heart filled with gratitude, and it is with immense appreciation that I acknowledge those who have made this thesis possible.

First and foremost, I extend my deepest gratitude to my advisor, Dr. Shoaib Usman, whose expertise and insightful guidance have been the lighthouses of my research challenges. His patience and scholarly rigor have not only shaped this work but also molded my development as an academic and a professional. The unconditional support and constructive criticism I received was invaluable and has left a significant mark on my growth.

I am deeply grateful to the thesis committee members Dr. Joseph Newkirk, and Dr. Syed Alam for their valuable insights and constructive critiques that have significantly enhanced the quality of this thesis. I am also indebted to Dr Ayodeji Alajo and Dr. Joshua Schlegel. Their collective wisdom and the nurturing academic environment they fostered have been pivotal in my scholarly pursuit. To the administrative and support staff, Angelica Hendrix within the department, thank you for your assistance throughout this process.

I must also express my boundless love and thanks to my parents, Sabina Akter, and Jalal Faryzi. Their unconditional love, unwavering support, and endless sacrifices have not only provided the foundation upon which I've built my aspirations but have also sustained me through the inevitable trials of academic life. Their belief in my abilities has been a source of motivation and resilience, for which I am forever indebted.

This achievement does not belong to me alone, but to all of us who have walked this path together. Thank you.

TABLE OF CONTENTS

Page

LIST OF ILLUSTRATIONS

PAPER I Page

PAPER II

LIST OF TABLES

PAPER I Page

PAPER II

1. INTRODUCTION

The safety and efficiency of nuclear power plants hinge on the reliable performance of numerous engineered safety systems, which must operate flawlessly under complex conditions. At the heart of these safety systems lies the necessity to understand and control the thermal-hydraulic phenomena that control reactor operation and safety (Bhowmik et al., 2022; Liao et al., 2016). Computational Fluid Dynamics (CFD) has emerged as an important tool for the analysis of these phenomena, allowing researchers and engineers to investigate the complexities of fluid flow and heat transfer within nuclear reactors (Kutbay & Şentürk Lüle, 2023; Podila et al., 2023; Song et al., 2018). This thesis presents an extensive study employing CFD to examine the thermal-hydraulic behavior in nuclear research reactors and the underlying mechanisms governing emergency core-cooling systems (ECCS) and gravitational heat pipes.

This work is structured in the form of a manuscript-based thesis, comprising detailed investigations to enhance our understanding of flow and heat transfer processes in nuclear reactor systems. The first paper focuses on utilizing the CFD tool FLUENT to analyze thermal-hydraulic behavior in two distinct reactor types: the Replacement Research Reactor (RRR) and the Missouri University of Science and Technology Reactor (MSTR). The RRR, operating at 20 megawatts with flat plate fuel assemblies, and the MSTR, exploring a hypothetical power uprate from 0.2 to 2 megawatts using curved plate assemblies, serve as the principal subjects of study. The paper addresses the complexity of flow in these configurations, providing insights into pressure drops, temperature profiles,

and the suitability of various modeling approaches, including both realistic and porous media simulations.

The second study focuses on the dynamics of multi-phase (liquid-gas) and multi-fluid (air-water, water-silicone oil) flows under varying wall wettability conditions in sealed environments, crucial for thermal management in industrial applications. Utilizing computational fluid dynamics (CFD) simulations and the volume-of-fluid (VOF) method with sharp interface modeling, it examines the influence of contact angle, channel size, gravity, and fluid viscosity on flow patterns and blockage. This comprehensive modeling approach aims to understand the complex interactions affecting flow behavior in closed channels. The research's objective is to inform design and analysis strategies for components like heat pipes and cooling systems in critical applications, such as emergency core cooling in nuclear reactors.

In both studies, CFD stands as an important investigative tool, allowing for the prediction and analysis of complex fluid dynamics that are otherwise difficult to study experimentally. As the global energy landscape shifts toward low-carbon sources, the demand for nuclear energy is expected to grow, accompanied by strict safety requirements. The design and optimization of nuclear reactors, therefore, requires a profound understanding of thermal-hydraulic processes to ensure operational safety and resilience against potential failures. This work not only advances our knowledge in this field but also provides a foundation for future investigations aiming to further improve reactor systems.

This introduction sets the stage for a comprehensive exploration of thermal-hydraulic analyses in nuclear reactors using advanced CFD techniques. The subsequent chapters will discuss the methodologies employed, the results obtained, and the implications of these findings for the design and safety of nuclear reactors.

PAPER

I. POROUS MEDIA MODEL SIMULATES THERMAL-HYDRAULICS OF NUCLEAR RESEARCH REACTORS WITH FLAT AND CURVED PLATE FUEL ASSEMBLY

Mehedi Hasan Tusar[1], Palash K. Bhowmik[1,2], Kazuma Kobayashi[3], Syed Alam[3], Shoaib Usman[1]*

[1] Department of Nuclear Engineering and Radiation Science, Missouri University of Science and Technology, Rolla, MO 65409, USA

[2] Department of Irradiation Experiment and Thermal-hydraulics Analysis, Idaho National Laboratory, Idaho Falls, ID 83415, USA

[3] Department of Nuclear, Plasma & Radiological Engineering, University of Illinois at Urbana–Champaign, Urbana, IL 61801, USA

ABSTRACT

The advancement of nuclear research reactors hinges on precise thermal-hydraulic analyses, especially when reactors undergo potential design modifications or power uprates. This study uses the computational fluid dynamics (CFD) tool, FLUENT, to analyze thermal-hydraulic behavior in the Replacement Research Reactor (RRR) and the Missouri University of Science and Technology Reactor (MSTR). The RRR model operates at 20 megawatts (MW) with flat plate fuel assemblies, while the MSTR explores a hypothetical power uprate from 0.2 to 2 MW using curved plate assemblies. Two CFD methods—realistic and porous media modeling—are applied for thermal-hydraulic analysis in RRR and MSTR. For RRR, realistic simulations at 5.08 m/s led to a 245 kPa pressure drop. In MSTR, simulations across 0.25–1.25 m/s velocities yielded maximum fuel and fluid temperatures of 323K and 303K, respectively, at 0.25 m/s and 2 MW power.

The determined inertia resistance factors are 9.81 m^{-1} (RRR), 12.35 m^{-1} (MSTR), and viscous resistance factors are 1.98 x 107 m^{-2} (RRR), 683060 m^{-2} (MSTR). This study validates porous media modeling as a computationally efficient approach for thermal-hydraulic analysis in nuclear reactors, effectively complementing realistic simulations for in-depth assessments.

Keywords. flat plate fuel, porous media modeling, FLUENT, research reactor, thermal hydraulics.

1. INTRODUCTION

Nuclear research reactors are incredibly important for education, training, research, and development of the nuclear industry. They are used in isotope production, materials testing, and many other applications (Mira et al., 2023; Morselli et al., 2023; Steiner et al., 2022; Wakabayashi et al., 2023). The primary goal of the research reactors is the production of neutrons in the thermal, epithermal, and fast neutron range. Thermal neutrons are utilized in neutron activation analysis, neutron radiography, isotope production, and irradiation experiments (Akyurek & Usman, 2015; Yasuda et al., 2022). However, fast neutrons or hard spectra are required for fast neutron damage analysis of irradiated materials, which is the scenario of advanced fast neutron spectrum reactors. Many of the research reactors operate in the thermal range of the neutron spectrum, while providing design support to operate the reactors in the fast spectrum. It is difficult to maintain fast neutrons in a highly moderated environment, but a single research reactor that can operate on both thermal and fast regime will provide flexibility and high-frequency of experimentation that is lucrative for commercialization as well (Alhuzaymi et al., 2023).

Therefore, neutronic and thermal-hydraulics study needs to be done for design and operation performance with safety analysis whenever a change in the reactor core configuration is needed (Hedayat & Davari, 2022).

The heat generation of nuclear reactors increases with a corresponding neutron flux increase. Neutron hits the U-235, which produces fission that generates heat. This heat raises the temperature of the fuel plates. Therefore, the removal of heat by coolant is necessary to sustain a safe steady-state operation of the core. Most of the nuclear research reactors are an open pool type and water is coolant. Low power producing reactor cores are cooled by natural convection through the reactor core (Bae & Bean, 2022). Boiling or excessive temperature rise should be avoided on pool water. Therefore, forced circulation of water is needed for research reactors with high-thermal power to control the fuel rod temperature at design limit (Umar et al., 2023). Computational fluid dynamics (CFD) is widely used for thermal-hydraulics analysis of the reactors in design, operation, and accident scenario analysis (Bhowmik & Schlegel, 2023). Nuclear reactor core involves multiphysics phenomenon that includes neutronics, thermal-hydraulics, material, and structural analysis. A pressurized water reactor core consists of 150 fuel assemblies, where every assembly has 289 regularly spaced rods. The fuel rods have a length of 4 m and a diameter of 1 cm. They are supported by guide tubes and spacer grids. The flow happens at 5 m/s axial velocity, which results in the Reynolds number, Re, to be 500000 (Ricciardi et al., 2009). The large-scale complex domain and higher heat transfer surface area in the turbulent flow regime makes it extremely computationally expensive. This is also a hindrance of accelerated design and testing of advanced nuclear reactors. So, researchers tried to perform system level thermal-hydraulics to cut out computational cost and time

(Zhang, 2020). Based on this CFD study of thermal-hydraulics is categorized into two segments attributed as realistic and porous media models (Mahaffy et al., 2007). The realistic approach studies the actual complex geometry of nuclear reactors (Jareteg et al., 2014). Wang et al. performed flow and heat transfer characteristics analysis of 5 × 5 fuel rod bundles with spacer grids via CFD simulation (Wang et al., 2020). Realistic CFD provides flexibility and faster results for nuclear systems, which are difficult to experiment with as well. Yan et al. (B. H. Yan et al., 2011) performed turbulent heat transfer analysis of rectangular channels in ocean conditions using FLUENT. Though computationally expensive, high-fidelity large eddy simulation of turbulent mixing in highly compact rod bundles was simulated (Ju et al., 2019). This realistic approach is also used in the CFD study of the complex pebble arrangement of pebble bed reactors as more accuracy can be achieved with this method for anisotropic thermal-hydraulics property evaluation in the longitudinal and transverse direction (Ahmed et al., 2021; Wu et al., 2010). Pebble bed reactors contain hundreds of thousands of pebbles in the core. The absence of a subchannel raises complexity in the application of the subchannel codes. Though realistic simulations offer high-fidelity, the higher computational cost shifts the attention towards a medium-fidelity porous media modeling approach. Porous media models will capture average thermodynamic properties of solid and fluid phase that is suitable for engineering scale analysis (Ge et al., 2016). Zou et al. (Zou et al., 2018) prepared a porous media model using the recent update of Pronghorn that is capable of accurate prediction with the SANA experiment. During the modeling of reactors using a porous media approximation, some new parameters were generated. These parameters are identified from benchmark studies or experiments. Friele et al. (Freile et al., 2021) performed high-fidelity simulations of

reactor cavity cooling and made it applicable for porous media modeling using Pronghorn. Yan and Rizwan (Y. Yan, 2011) constructed a porous media model of the Replacement Research Reactor (RRR) of the Australian Nuclear Science and Technology Organization (ANSTO) running at 20 MW power, cooled by forced circulation (Cameron & Horlock, 2001). Also, Sipaun and Usman (Sipaun & Usman, 2015) developed a porous media model of the Missouri University of Science and Technology Reactor (MSTR) operating at 0.2 MW power for natural circulation.

There are lots of interests and activities worldwide going on for advanced fuel, material, and advanced reactor systems. Particularly after the Fukushima Daiichi nuclear power plant accident in 2011, the United States (U.S.) Department of Energy–Office of Nuclear Energy (DOE-NE) initiated the enhancement of accident tolerance of light water reactors (LWRs) under the 2012 Consolidated Appropriations Act, Conference Report 112-75, by the U.S. Congress (Carmack et al., 2013). This accelerated the research and testing of new reactor concepts, accident tolerant fuel (ATF) claddings, and advanced fuels. SiC/SiC, FeCrAl, and coated Zr-based cladding are tested as ATF claddings for next generation and existing reactors (Terrani, 2018). Advanced fuels like UN, U3Si2, U3Si5, TRIstructural isotropic (TRISO), and ThO2 fuel kernels are also tested in nuclear reactors (Yun et al., 2021). Research reactors are used to perform the fuel and material qualification, but need necessary reactor power, neutron flux, and testing capacity. At present, fuel and material qualification testing in the U.S. are performed by the High Flux Isotope Reactor (HFIR), the Advanced Test Reactor (ATR), and the Transient Test Reactor (TREAT). However, these reactors have gone through several decades of operation and because they go from a conversion of high-enriched fuel to low-enriched fuel, long outages occur.

University research reactors may be able to support fuel and material qualification, but they need preparedness like power uprate, testing capabilities, and regulatory approval, such as the U.S. Nuclear Regulatory Commission (NRC) and the U.S. Department of Energy (DOE) for the U.S. reactors mentioned above. MSTR now operates on low-enrichment fuels. Power uprates of MSTR are needed to facilitate higher neutron flux in the reactor. Therefore, a thermal-hydraulics study needs to be performed in the forced convection heat transfer regime.

Considering the prior discussion regarding the computational efficiency of porous media modeling of nuclear reactors, this study will computationally investigate thermal-hydraulics in realistic flat plate fuel assemblies (FAs) of the RRR. The inertial and viscous resistance factors, which are the two most important parameters in porous media modeling, will be identified. The operation of nuclear research reactor cores will be computationally evaluated in forced convection mode where the reactor core will be replaced by porous media with a volumetric heat source. The temperature field and pressure drop in the core will be evaluated. The computational models will be validated against the benchmark study. Then, we will perform a feasibility study of power uprate to 2 MW of MSTR in forced convection regime. Our validated model will be used for realistic modeling of FAs with the MSTR curved fuel plate. Inertial and viscous resistance factors will be determined for porous media modeling. Finally, we will evaluate different power uprate conditions implementing volumetric heat source and check its effect on temperature and pressure field in the core and reactor pool. ANSYS FLUENT, a commercial software package, will be used.

2. OVERVIEW OF THE MSTR

The MSTR is cooled by natural convection. In 2012, a secondary heat exchanger system was installed to remove heat from pool water for continuous operation of the core (Castano Giraldo et al., 2013). MSTR uses high-assay low-enriched uranium (HALEU) of 19.75% U-235 concentration in the form of uranium silicide. The fuel configuration is a curved flat plate. This core has a total of 310 MTR type fuel plates and 295 coolant channels. The details of the curved FA are described in Table 1. The reactor pool dimensions are 5.79 m × 2.74 m × 8.23 m in length, width, and depth, respectively. An overview and core configuration of MSTR core is given in Figure 1.

Table 1. Technical specifications for the MSTR core (Bonzer & Carroll, 2008).

Fuel Specifications	Value	Clad and Other Specifications	Value
Fuel meat thickness	0.51 mm	Cladding thickness	0.381 mm
Fuel meat width	61.0 mm	Plate thickness	1.27 mm
Fuel meat length	610 mm	Channel gap spacing	3.15 mm
Number of fuel plates	18	Fuel element total surface area	30 m^2

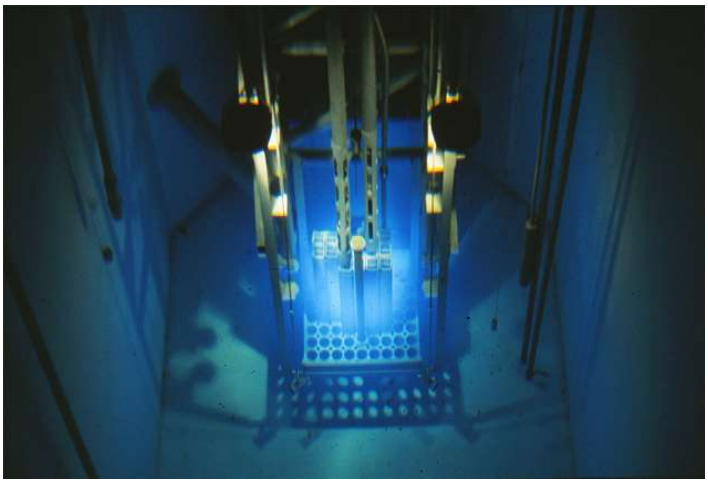

(a)

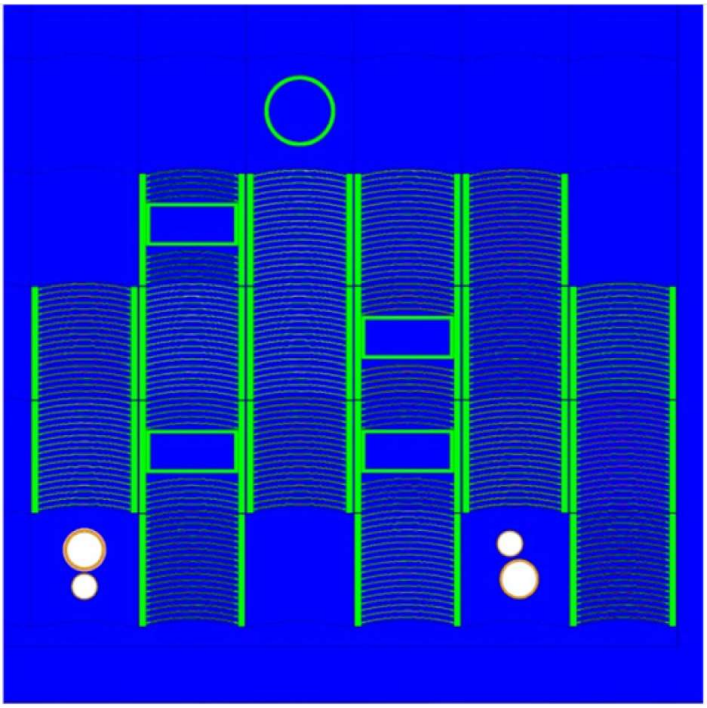

(b)

Figure 1. (a) Overview of the MSTR at full power. (b) Core configuration of MSTR (Richardson et al., 2012).

3. METHODOLOGY AND SIMULATION PROCEDURE

3.1. CALCULATION AND SIMULATION PREPARATION

First, we solved the adiabatic flow configuration for the FA and determined the pressure drop. Then, we approximated the porous media parameters with Equation 1. We could determine inertial and viscosity resistance factors, C2 and 1/α, respectively, as mentioned in Equation 2 and Equation 3. After determining the porous media parameters, we performed the simulation of the reactor core region as a porous zone with a volumetric heat source. A schematic diagram is depicted in Figure 2.

$$\frac{\Delta p}{\Delta x} = Av^2 + Bv \tag{1}$$

$$C_2 = \frac{2\,A}{\rho\,L} \tag{2}$$

$$\frac{1}{\alpha} = \frac{B}{\mu\,L} \tag{3}$$

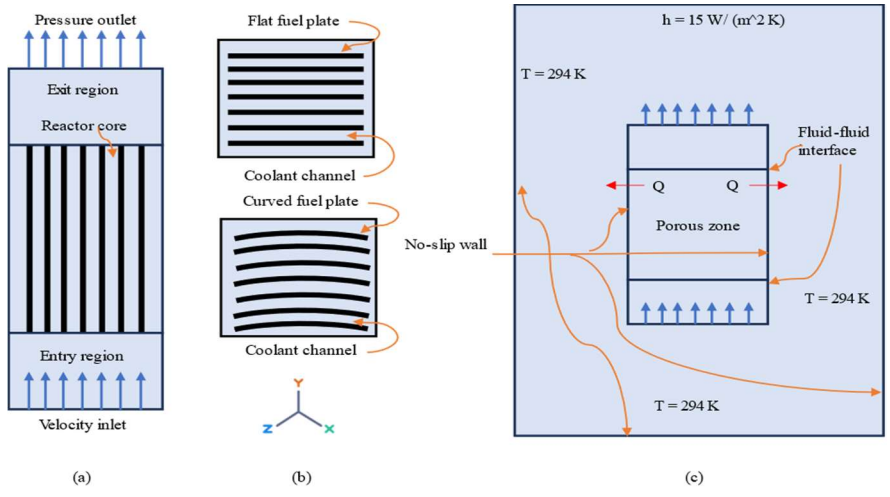

Figure 2. Schematic of (a) front view of realistic core; (b) FA cross section; and (c) reactor pool with core modeled as porous media.

We then checked the thermal-hydraulics aspects, such as pressure drop, temperature, turbulence kinetic energy (TKE), etc. Every geometry was designed in SOLIDWORKS. The designed geometry was imported into ANSYS FLUENT as an STL file. The fuel domain was removed though the Boolean cut in realistic simulation for the flat plate FA. This removal drastically reduced the total mesh element and saved computational time. The fuel plates were replaced by heat flux walls corresponding to the thermal power conditions. The entry and exit region of the FA was discretized with a 4 mm face size mesh element, since they did not have closely packed fuel plates or an abrupt variation in the flow field. The reactor core with closely packed fuel plates were meshed with 2 mm grids using a sphere of influence method that covers a length of 100 mm of the entry and exit region adjacent to the reactor core for capturing the entrance and exit effect. The ANSYS mesh modeler was used for meshing. Later, the resulting combination of tetrahedral and prism mesh was converted into polyhedral mesh as it provides a lower amount of mesh element, flexibility in conforming to complex geometries, reduced computational time, and good accuracy (Sosnowski et al., n.d.). The resultant domain had 2.37 million polyhedral cells. We replaced the reactor core with heat flux walls by a reactor core as porous media when the overall reactor pool simulations were performed. The heat transfer from the fuel plate walls to the flow medium was happening at thermal equilibrium. A volumetric heat source was implemented for the RRR core, which has a volume of 0.075 m^3. The flow happens in a vertically upward direction for forced circulation condition. The water was entering and exiting the porous domain via a fluid-fluid interface. The generated heat from the core is propagating in the longitudinal direction carried away by flow. Heat diffusion in the transverse direction is also considered in this simulation. Therefore, the

core boundary walls of an Al plate were modeled as no slip, and the thermally coupled wall for momentum and the thermal boundary condition. The reactor water at the pool boundary was at an ambient temperature of 294 K. Figure 2(c) provides the visualization of the pool with boundary conditions. Similar procedures are followed for MSTR core simulation.

3.2. GOVERNING EQUATIONS AND SOLUTION PROCEDURE

3.2.1. Realistic Modeling. FLUENT is a powerful tool for computational modeling of single and multiphase flow for a wide range of Re from laminar to turbulent flow. In this finite volume method of flow simulation, it only solves the continuity and momentum equations, respectively, as described in Equation 4 and Equation 5, respectively, when no energy or phase change is involved.

Continuity equation:

$$\frac{\partial \rho}{\partial t} + \nabla \cdot (\rho \vec{v}) = S_m \tag{4}$$

where ρ, $\vec{v}$, and S_m are density, velocity, and mass source term in the flow domain.

Momentum equation:

$$\frac{\partial}{\partial t}(\rho \vec{v}) + \nabla \cdot (\rho \vec{v} \cdot \vec{v}) = -\nabla p + \nabla \cdot (\bar{\bar{\tau}}) + \rho \vec{g} + \vec{F} \tag{5}$$

where p, $\bar{\bar{\tau}}$, $\rho \vec{g}$, and $\vec{F}$ are static pressure, stress tensor, gravitational, and external body force term, respectively. The stress tensor, $\bar{\bar{\tau}}$, is defined as Equation 6, where μ and $\bar{\bar{I}}$ are viscosity and unit tensor, respectively.

$$\bar{\bar{\tau}} = \mu \left[(\nabla \vec{v} + \nabla \vec{v}^T) - \frac{2}{3} \nabla \cdot \vec{v} \cdot \bar{\bar{I}} \right] \tag{6}$$

It additionally solves the energy equation described in Equation 7 when heat transfer is also involved in the boundaries of the system.

Energy equation:

$$\frac{\partial}{\partial t}(\rho E) + \nabla \cdot (\vec{v}(\rho E + p)) = \nabla \cdot \left(k_{\text{eff}} \nabla T - \sum_j h_j \vec{J}_j + \left(\bar{\bar{\tau}}_{\text{eff}} \cdot \vec{v} \right) \right) + S_h \quad (7)$$

where k_{eff}, h_j, and $\vec{J}_j$ are effective thermal conductivity, enthalpy, and diffusion flux of a particular species, j, respectively. S_h is the volumetric heat source.

The parameters of the Navier-Stokes Equation are dependent on turbulence. Our simulation was performed for RRR and MSTR at forced convection regime. For operating conditions, the velocity on the core is 8.2 m/s, which is the turbulent flow condition.

3.2.2. Porous Media Modeling. FAs are a consecutive arrangement of fuel plates surrounded by coolant channels that are ideal candidates for porous media modeling. We used porosity, γ, which is the ratio of fluid volume to that of total volume. In the coolant channel, the physical velocity was higher than the physical velocity at the entry region as it had a lower flow cross-section. When porous media approximation was performed, we considered the whole region to be a fluid domain where momentum drop was calculated by the negative source term. Therefore, superficial velocity was calculated in the core region with Equation 8. The equation of mass or continuity (e.g., Equation 9), momentum (e.g., Equation 11), and energy (e.g., Equation 12) of porous media flow were similar in pattern to the realistic modeling after accounting the effect of porosity.

$$\vec{v}_{\text{superficial}} = \gamma \vec{v}_{\text{physical}} \quad (8)$$

Mass conservation equation:

$$\frac{\partial(\gamma\rho)}{\partial t} + \nabla.(\gamma\rho\vec{v}) = 0 \tag{9}$$

There is an added momentum source (e.g., Equation 10) in the momentum equation for porous media flow. The negative sign indicates the drop in momentum. This momentum source is composed of inertia and viscous force components. The viscous component in 1/α form (α is permeability) and the inertia component, Cd, are used in the procedure.

$$S_i = -\left(\frac{\mu}{\alpha} v_i + C_d \frac{1}{2} \rho |v| v_i\right) \tag{10}$$

Momentum conservation equation:

$$\frac{\partial(\gamma\rho\vec{v})}{\partial t} + \nabla.(\gamma\rho\vec{v}\vec{v}) = -\gamma \nabla P + \nabla.(\gamma\vec{\tau}) + \gamma\overrightarrow{B_f} - \left(\frac{\mu}{\alpha} + C_2 \frac{1}{2} \rho |\vec{v}|\right)\vec{v} \tag{11}$$

Energy conservation equation:

$$\frac{\partial}{\partial t}(\gamma\rho_f E_f + (1-\gamma)\rho_s E_s) + \nabla.\left(\vec{v}\,(\rho_f E_f + P)\right) = \nabla.\left[K_{eff}\nabla T - (\textstyle\sum_i h_i J_i) + (\bar{\bar{\tau}}.\vec{v})\right] + S_f^h \tag{12}$$

Where E_f, E_s, K_{eff}, and S_f^h are total fluid energy, total solid medium energy, effective thermal conductivity of the medium, and fluid enthalpy source term, respectively. Ks and Kf are the solid and fluid medium conductivity, respectively, which includes turbulent contribution, kt, as given in Equation 13.

where E_f, E_s, K_{eff}, and S_f^h are total fluid energy, total solid medium energy, effective thermal conductivity of the medium, and fluid enthalpy source term, respectively. Ks and Kf are the solid and fluid medium conductivity, respectively, which includes turbulent contribution, kt, as given in Equation 13.

$$K_{eff} = \gamma K_s + (1 - \gamma) K_f \tag{13}$$

3.2.3. Solver Setup. The steady-state solution was performed for all configurations. The coupled scheme was used for pressure velocity coupling. The least square cell-based method was used for gradient spatial discretization. The pressure, momentum, TKE, specific dissipation rate, and energy are solved using second order upwinding. There is an entry region, core, and exit regions in realistic modeling for flat FA. The curved FA also possesses curved surfaces. Therefore, the warped face gradient correction was also used. Relaxation factors were set to 0.5 for pressure and momentum, 1 for density and body forces. The continuity, velocity, k, and ω residuals are set to 10^{-3}, whereas energy was set to 10^{-6}. The solution is solved till it reaches the residual limit. The parameter set method was used to perform parametric analysis where velocity and volumetric heat source were used as the input parameters. Pressure at the inlet, core entry, and exit point were used as output parameters. This setup reduces manual solving for every input parameter as it solves all the input parameters in a single simulation for the desired output parameters. 16 logical cores of Intel Core i9-10900 central processing unit (CPU) with a 2.8 GHz clock speed were used for parallel processing in this study. It uses ANSYS FLUENT software from Missouri University of Science and Technology server.

4. RESULTS

4.1. GRID TEST AND VALIDATION

The grid test and validation were performed for flat plate FA to check the required number of mesh elements for obtaining grid independent results. We used a 1.5 mm, 2 mm, and 3 mm mesh size for the flat plate FA simulation. The discretized domains are shown in Figure 3. An inlet velocity of 5.08 m/s was implemented in the lower plenum of the entry region of the FA. Longitudinal static pressure for the above-mentioned mesh sizes is plotted in Figure 4. It is measured as the mass flow average property across the cross section in the longitudinal direction. The result was found to be insensitive in the implemented grid size range. Therefore, we used the 3 mm grid size for the flat and curved FA modeling, respectively. A validation study followed the grid test. The RRR benchmark data was reproduced for validation and study of Yan and Rizwan for comparison (Cameron & Horlock, 2001; Y. Yan, 2011). Figure 5 shows that the RRR had a pressure drop of 240 kPa across the FA for an inlet velocity of 5.08 m/s. Yan and Rizwan (Y. Yan, 2011) performed a realistic and porous media simulation of RRR with a standard k-ϵ turbulence model with an enhanced wall treatment. They reported a 180 kPa pressure drop for the same test. They claimed that the difference in this result was made by local pressure drops of supporting core structure that was ignored in the simulation. In the current study, we made some changes to simulate the RRR FA. We used the Standard k-ϵ turbulence model with a standard wall treatment. Additionally, we considered curvature, corner flow, low Re correction, and considered surface roughness of the fuel plates. We found a pressure drop

of 245 kPa for the same test. Because of the close match with the benchmark data, we followed the same model for the flat and curved plate FA modeling.

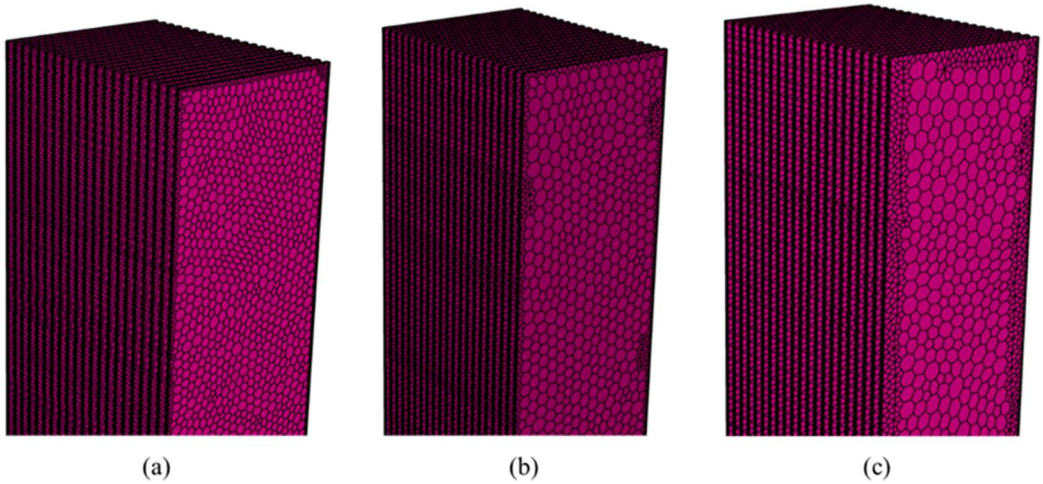

Figure 3. Discretized mesh domain with different grid sizes (a) 1.5 mm (b) 2 mm (c) 3 mm.

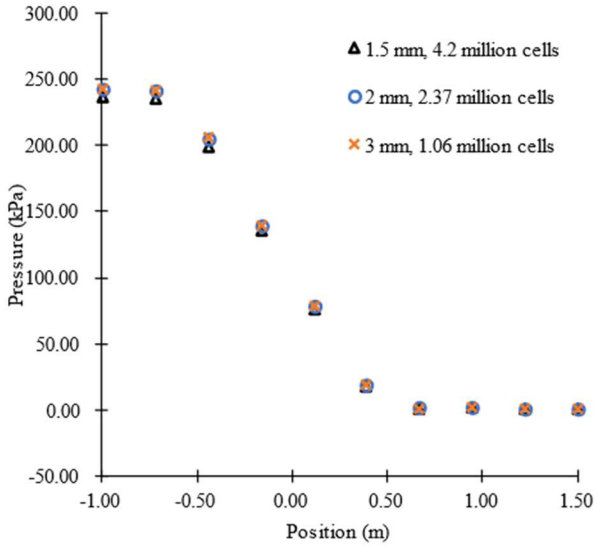

Figure 4. Grid test.

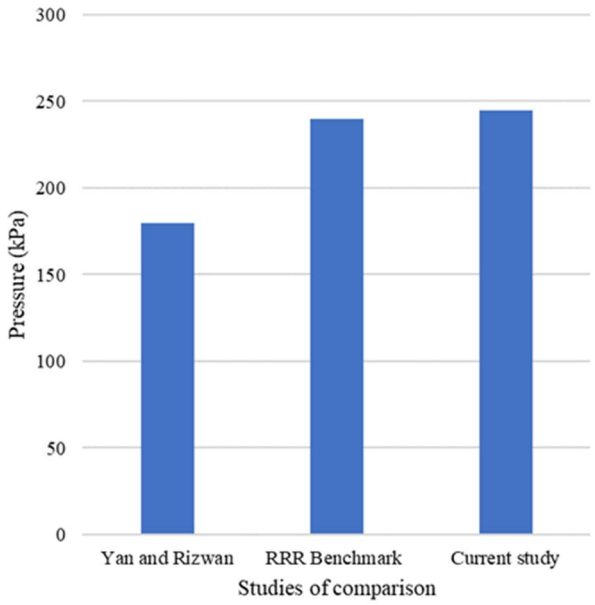

Figure 5. Validation study.

4.2. FLAT PLATE FUEL ASSEMBLY MODELING

Longitudinal static pressure for realistic, porous media adiabatic, and porous media with a heat source were investigated and plotted in Figure 6. Flow happened through thin rectangular channels in realistic flow. It generates secondary flow created by turbulence produced as an anisotropy of normal stresses (Menter et al., 2021). The eddy-viscosity models couldn't not represent this effect. Therefore, quadratic closure relationship proposed by Spalart (Spalart, 2000) was used to extend the eddy-viscosity model. The results were more accurate with the benchmark using this model. After finding the pressure drop for realistic simulation, we have determined the inertial and viscous resistance factor as described in the methodology section using Equations 1 through 3. Pressure drop data was fitted with equation 1 and the coefficient 'A' and 'B' are extracted for the best fit line. Equation 2, and 3 are used to find the inertial resistance factor, C2 and viscous resistance factor, $1/\alpha$. We found the inertial resistance factor, C2, and the viscous resistance factor,

$1/\alpha$, to be 9.8 m^{-1} and 1.98 x 10^7 m^{-2}, respectively. These parameters were implemented along with a porosity of 0.68 in the porous media model as the fuel assembly provides 68 percent coolant flow cross section of total cross section. The static pressure was higher, or the pressure drop was lower, in the porous media approximation as observed in the current study. This was caused by the unavailability of the no slip walls that promoted turbulence, which caused the pressure drop. It was also observed that static pressure data were different than the benchmark study if the RANS model accommodated low Re, corner, and curvature flow correction. Since the complex geometry was replaced by porous media, there was no need for this correction, which would have overestimated the pressure drop. We used appropriate heat flux at the fuel wall to replicate the thermal power scenario of 10 MW and 20 MW. Viscosity and thermal expansion of water, two temperature-dependent phenomena were observed to affect pressure drop since the temperature-dependent thermodynamic properties were considered in the simulation. The viscosity decreases with temperature; therefore, the pressure drops decreases with a rise in power. Whereas the thermal expansion of water with a rise in temperature increases the volumetric flow rate and pressure drop accordingly. As a combined effect, static pressure was observed to decrease with increasing thermal power.

Figure 7 describes the local surface temperature of fuel rods and bulk fluid temperature in the longitudinal direction. We got the precise data for a localized temperature in realistic modeling for fluid and solid, whereas only bulk-averaged solid-fluid temperature data was available in porous media modeling. A difference of temperature in the realistic and porous media model was also observed in another study (Zou et al., 2018). The active fuel length was 615 mm embedded in an Al plate extrusion

on both the entrance and exit sides. There was thermal diffusion of heat in the inactive region of fuel rod on both the active and exit sides. So, fuel rod temperature was observed to rise in the inactive region as well. We used equivalent volumetric heat sources of 133 MW/m^3 and 266 MW/m^3 in replacement of FA in porous media modeling for 10 MW and 20 MW power simulation. It was expected to see a higher wall and bulk fluid temperature for the rise in power at the same flowrate. The surface temperature at the FA outlet was 301.3 K and 308.635 K for 10 MW and 20 MW power, respectively. The bulk fluid temperature was 297.8 K and 301.7 K. The bulk temperature in porous media modeling was a close match with the realistic modeling. Some hotspots of elevated temperature were also observed across the FA, which is difficult to monitor with an experimental study. The highest temperature point in the assembly was determined to be 313.8 K and 333.5 K for 10 MW and 20 MW power, respectively. Figure 8 demonstrates local temperature, velocity, and TKE cross-section wise at the FA inlet, middle, and outlet. In the inlet or entrance region, flow velocity was 5.08 m/s, which increases in the FA as the flow cross-section reduces by the position occupied by the fuel rods. A velocity of 7-8 m/s was observed in this range, which reduces to 5.08 m/s in the exit region. The local velocity was higher between the support structure and coolant channel because of the least resistance. It was lower adjacent to the fuel walls because of no slip. The temperature field was dependent on the velocity field at positions besides heat generation. We observed the temperature to be highest in the thermal boundary layers and in the low velocity regions. Comparable results were also observed in other studies (M. Tusar, Ahmed, et al., 2019; M. Tusar, Noman, et al., 2019; M. H. Tusar et al., 2021). The TKE at the inlet was zero, but it was developed in the FA by buoyant, thermal, and mechanical generated eddies—the

maximum of which reached 2.3 m^2s^{-2}. Figure 9 shows the solid-fluid averaged temperature, velocity, and TKE contour at the outlet for porous media modeling. These parameters were observed to be homogenous radially due to uniformity approximation. However, with higher resolution it is understandable to observe local variations of properties. The TKE was observed to be almost zero except for the corners because the mechanical eddies were absent in this modeling due to the replacement of fuel plate walls. Higher velocity increases swirl, therefore producing TKE. This energy dissipates as thermal energy, raising the temperature of that region. Though the eddy-related pressure drop is accounted in the momentum equation by inertial and viscous resistance factor, it is not observable in this modeling method.

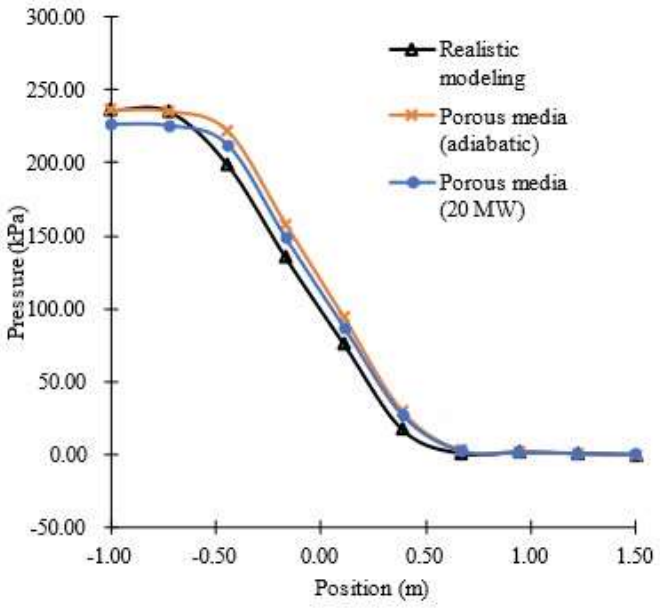

Figure 6. Longitudinal static pressure profile for flat plate FA.

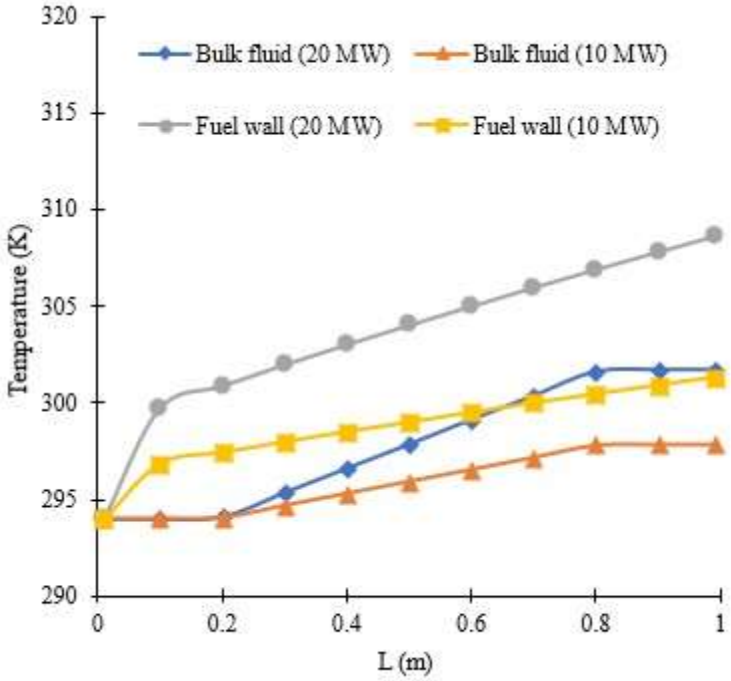

Figure 7. Longitudinal temperature profile for flat plate FA at v = 5.08 m/s.

4.3. CURVED PLATE FUEL ASSEMBLY MODELING

Figure 10 shows the fuel surface temperature in the longitudinal direction for a velocity of 0.25, 0.5, 0.75, 1.00, and 1.25 m/s at 2 MW power, respectively. The pool water temperature at the inlet was 294 K. The fuel surface temperature was 323.0, 311.0, 305.4, 302.4, and 300.6 K, respectively, at the outlet consecutively for the velocity range specified. The bulk fluid temperature at the outlet was 307.3, 300.6, 298.4, 297.3, and 296.6 K, respectively, accordingly. Since the bulk fluid temperature was much lower than the boiling point of water, it is expected to have a minor change in neutron moderation. A detailed neutronics study can be conducted to determine the effect of proposed uprate, which is outside of our current study. Also, the fuel temperature was much lower than the

safe operation temperature of MTR-type FA. As such, MSTR can safely operate at 2 MW power from the thermal-hydraulics point of view.

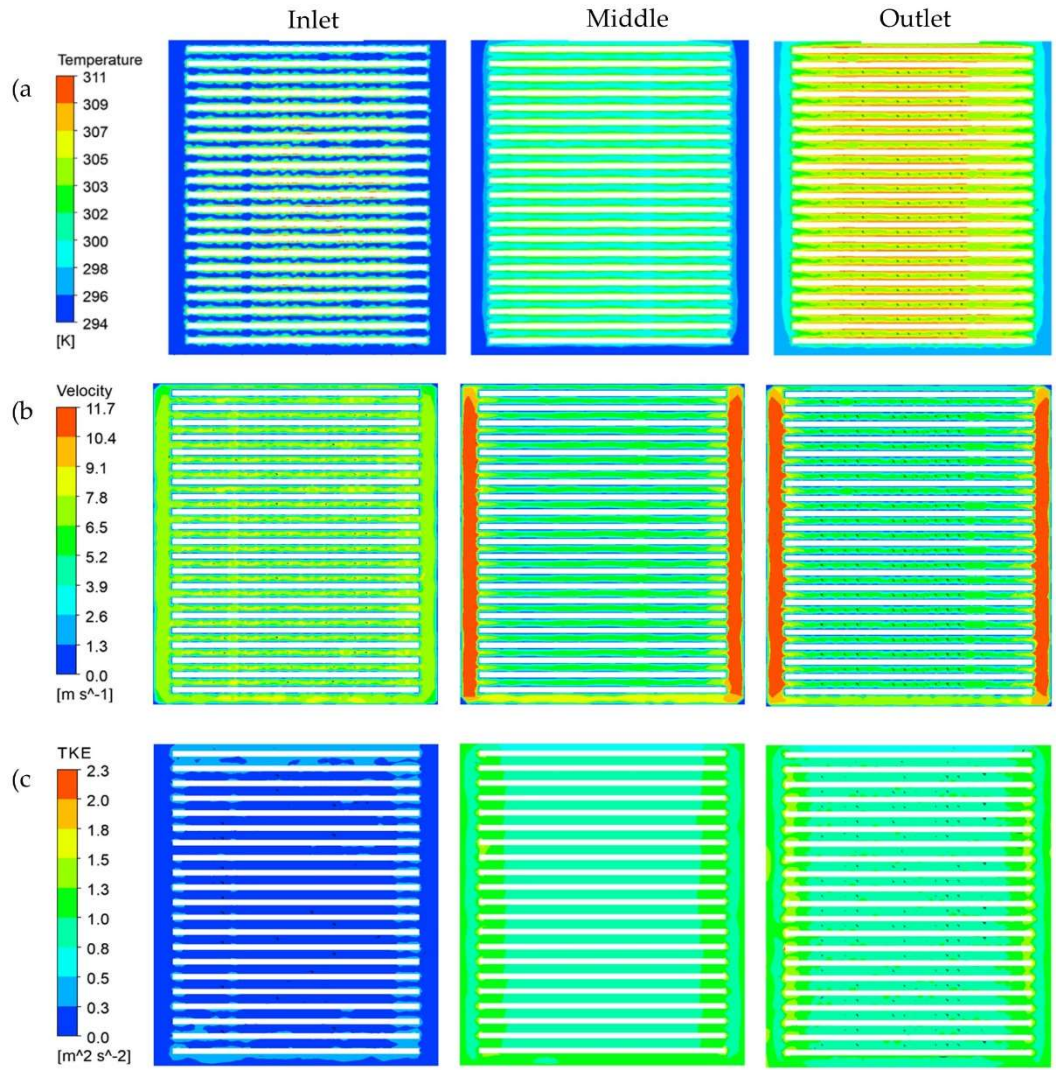

Figure 8. Realistic simulation contours at cross-sections for core power of 20 MW at 5.08 m/s inlet velocity for: (a) temperature distribution; (b) velocity distribution; and (c) turbulent kinetic energy distribution.

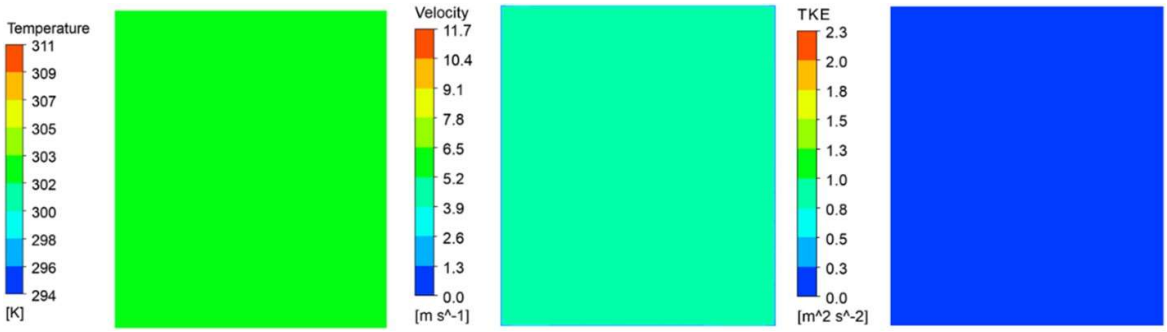

(a) (b) (c)

Figure 9. Porous media simulation contours at FA outlet for core power of 20 MW at 5.08 m/s inlet velocity for: (a) temperature distribution; (b) velocity distribution; and (c) turbulent kinetic energy distribution.

Pressure drop across the FA with respect to velocity was plotted in Figure 11. The rise in pressure drop was non-linear with velocity. A correlation, as derived from Equation 1, was developed with the least square method from the array of pressure and velocity data in the MATLAB software. Constants A and B are 3760 and 375, respectively. So, the inertial and viscous resistance factors were determined as 12.35 m^{-1} and 683060 m^{-2}, respectively, from Equation 2 and Equation 3. The coefficients determined are employed in the porous media modeling of curved plate FA with 0.7 value for porosity as the fuel assembly provides 70 percent coolant flow cross section of total cross section. Figure 12 represents static pressure for the realistic and porous media model. A close match was observed between them. It is expected to have the same effect on temperature, velocity, and TKE for the curved plate fuel as flat plate fuel. Figure 13 represents an isometric and cross-section view of the fuel surface and bulk fluid temperature profile. The fuel plates adjacent to the support structure had a lower temperature as it transfers heat into the pool water through the support structure. The plates in the middle had a higher temperature. It was also observed that locations at the peak of the curve plate had the lowest temperature

in the radial direction as the curve helps in secondary flow. In the case of a flat plate fuel design, the highest temperature typically occurs at the center. However, with a curved fuel design, this pattern changes; the highest temperature shifts radially towards the edge rather than being concentrated at the center. The viscosity decreases and the volumetric flow rate increases due to thermal expansion with a rise in thermal power. We observed the thermal power rise impact on volumetric flow rate in the longitudinal direction for 0.25 m/s velocity. The flowrate difference is 8 cc/s between the inlet and the outlet. From Figure 11, we observed an increase in velocity, thus flowrate, the increased pressure drops. The flowrate should be kept to a minimum when sufficient cooling can be provided by the circulated water. Therefore, 0.25 m/s velocity can be considered as forced convection velocity of the MSTR for the considered power uprate. The fuel surface temperature at the outlet was 297.2, 302, 309.7, 318.3, and 324.2 K, respectively, for thermal power of 0.2, 0.5, 1.0, 1.5, and 2 MW at 0.25 m/s velocity, respectively. The temperature profile is shown in Figure 14. There was a rise in temperature at the fuel inlet because of the entrance effect, which decreases with flow development. Then the temperature increased linearly. This temperature rises at the inlet due to the entrance effect, which might be ignored if the cosine heat flux profile is implemented as seen in nuclear reactors. We checked the effect of thermal power on pressure drop at 0.25 m/s velocity. It was 608, 605, 597, 588, and 583 pa/m, respectively, for 0.2, 0.5, 1.0, 1.5, and 2 MW power, respectively. The pressure drop was decreasing with a corresponding increase in thermal power for constant mass flow rate, as shown in Figure 15. However, the decrease was less than 5 percent, and therefore, it can be considered to have less significance to be included in inertial and viscous resistance factor determination. Finally, we performed a simulation for MSTR with 2 MW

thermal power at 0.25 m/s forced circulation across the core, where core was modeled as porous zone. Figure 16 shows the temperature profile of the reactor core. It is observed to have temperature below 373 K for steady-state operation, and the results are comparable with Sipaun and Usman (Sipaun & Usman, 2015).

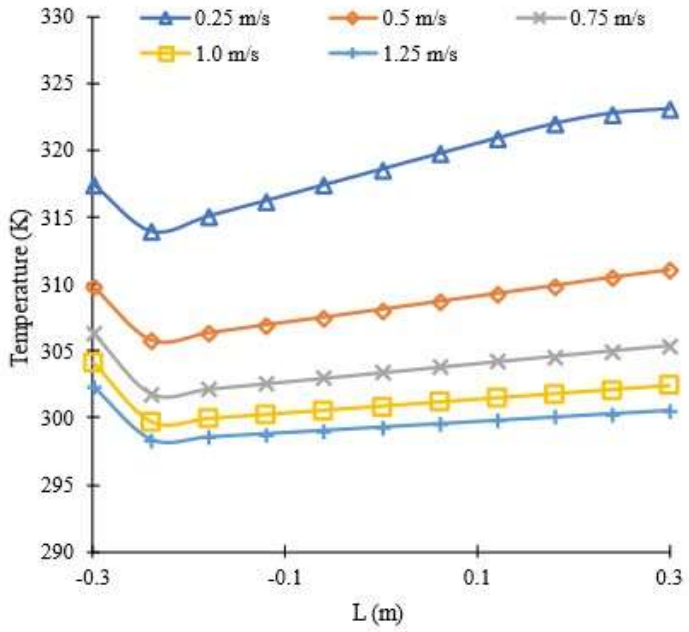

Figure 10. Temperature of the curved FA at 2 MW power.

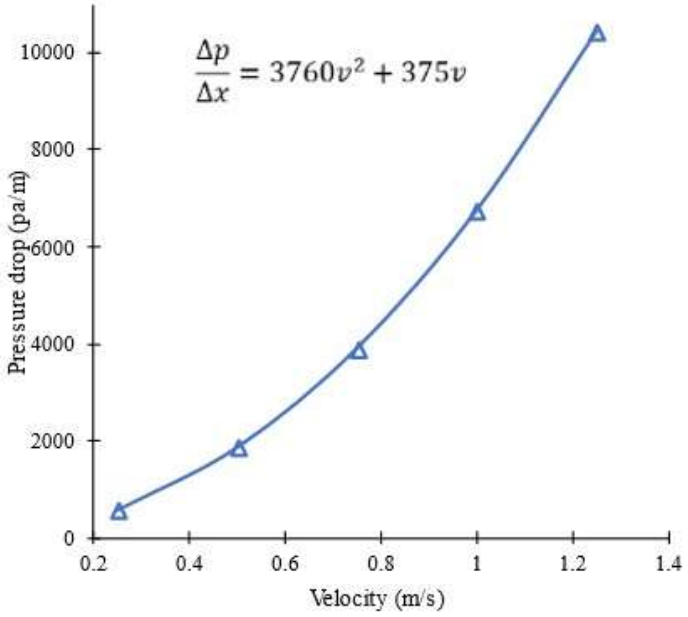

Figure 11. Pressure drops of the curved FA at 2 MW power.

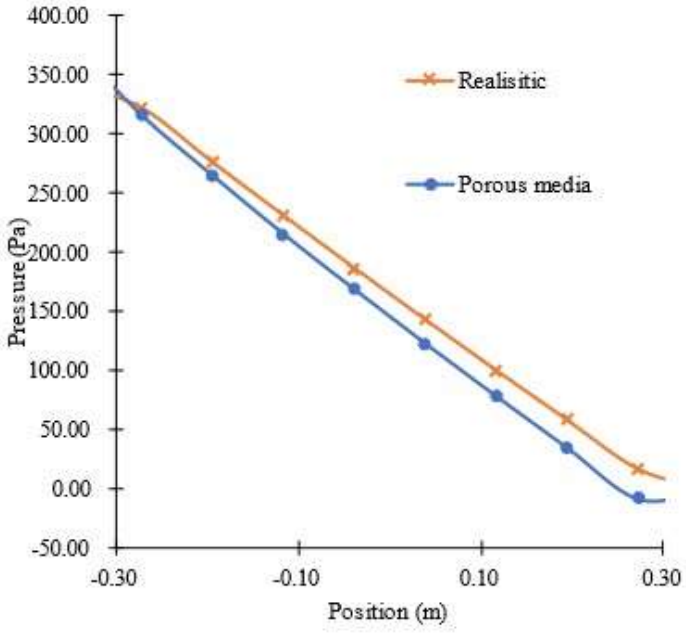

Figure 12. Longitudinal static pressure profile for curved plate FA at 2 MW power.

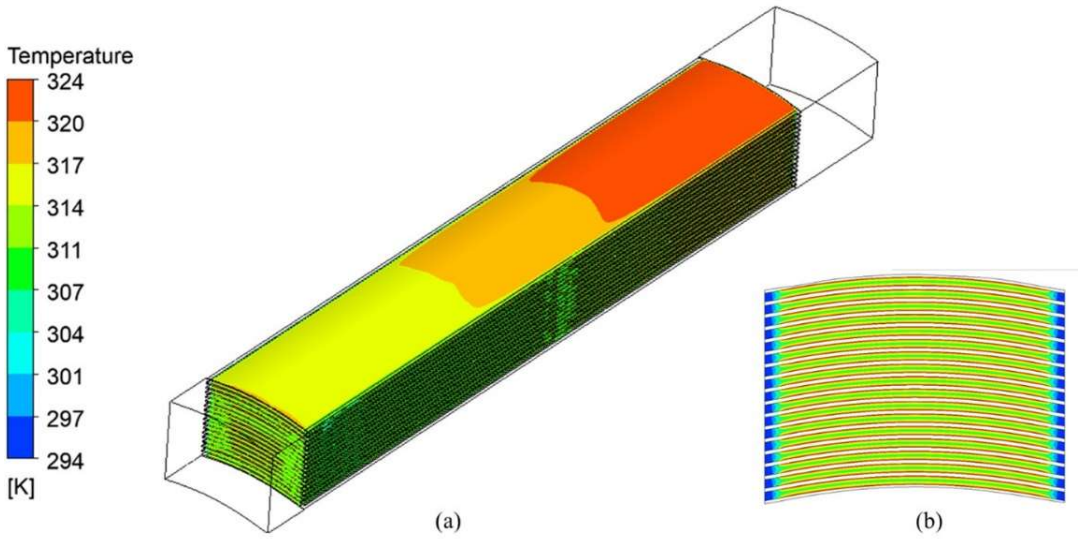

Figure 13. Temperature for (a) the curved FA, isometric view (b) bulk fluid, cross section view.

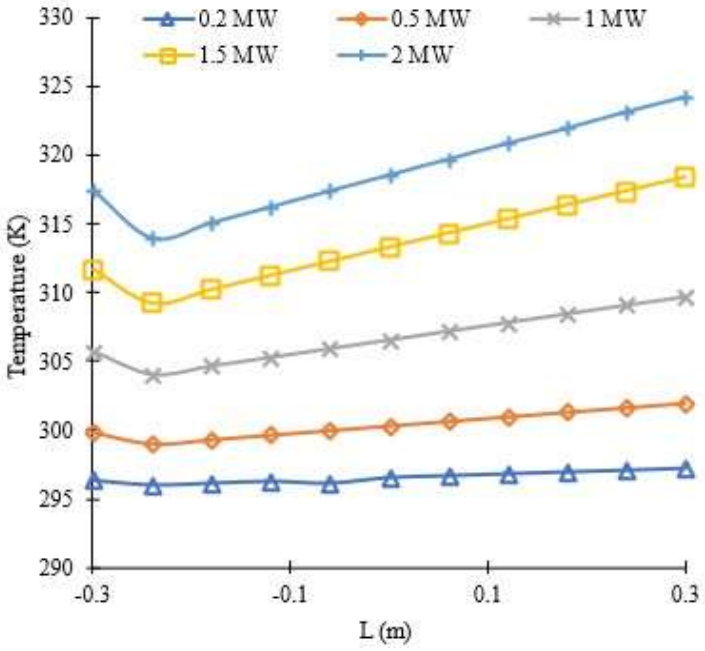

Figure 14. Temperature of the curved FA at 0.25 m/s coolant velocity at various power configuration.

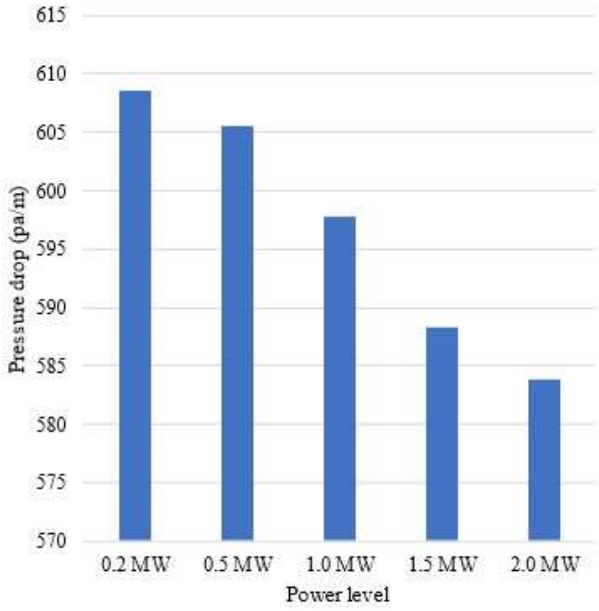

Figure 15. Pressure drops of the curved FA at 0.25 m/s coolant velocity at various power configurations.

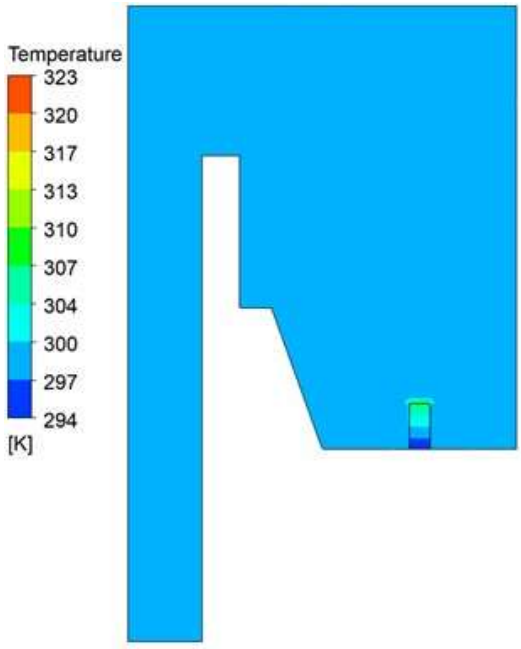

Figure 16. Simulation of the water pool with reactor core replaced by porous zone.

5. DISCUSSIONS AND CONCLUSIONS

The CFD study conducted a thermal-hydraulics analysis on both flat and curved plate fuel assemblies. The RRR had been studied for flat plate fuel assemblies and MSTR for curved plate fuel assemblies. Two different CFD approaches (i.e., realistic, and porous media modeling) were performed on both reactor cores as high- and medium-fidelity solution approach for thermal-hydraulics:

- A realistic simulation was performed for the RRR FA at 20 MW power for forced circulation of water at 5.08 m/s velocity.
- The pressure drop data across the FA was benchmarked, which was 245 kPa at the operating condition. The inertial and viscous resistance factors were curve-fitted from the pressure data, which was 9.81 m^{-1} and 1.98 x 10^7 m^{-2}, respectively.
- The porous media modeling of the reactor core is done applying these coefficients alongside the porosity of 0.68.
- The temperature and static pressure profile for both modeling was compared and found to be in good agreement. However, TKE was observed to be zero for porous media modeling due to the absence of no-slip walls that typically promote turbulence. The effect of eddies gets accounted for the porous media in momentum equation using a negative source term.

The application of curvature, corner, and low Re is necessary in realistic simulation, but should be ignored for porous media modeling to avoid overestimation of the pressure drop. A proposed power uprates of MSTR from 200 KW to 2 MW to facilitate high neutron fluence and fast spectrum were investigated for thermal-hydraulics safety analysis:

- The realistic simulations were performed for curved FA at 2 MW power in the water circulation velocity from 0.25 to 1.25 m/s through the FA with temperature-dependent physical properties.
- The highest temperature was 323 K and 303 K for fuel surface and bulk fluid at outlet for velocity of 0.25 m/s. In the curved plate FA, the influence of curvature on flow dynamics and temperature distribution was highlighted.
- The study found that the highest temperature points shift radially towards the edge in curved plate designs, unlike in flat plate assemblies where they occur at the center. Secondary flows generated by the curvature also contributed to this unique temperature distribution. Since the increase in water flow rate will increase pressure drop and cost, lower forced convection velocity is desired.
- The pressure drop vs velocity data is prepared in the Forchheimer equation and solved using the least square method for inertial and viscous resistance factor. They are 12.35 m^{-1} and 683060 m^{-2}, respectively.
- The porous media modeling of the reactor core is done applying these coefficients alongside the porosity of 0.7. The realistic and porous media simulations showed good agreement. The effect of thermal power on pressure drop for constant mass flow rate is evaluated. The pressure drop was observed to decrease with an increase in thermal power as viscosity decreases, which surpasses the rise in pressure drop due to volumetric expansion. However, the decrease is less than 5 percent; therefore, accommodation of this effect in porous media coefficients is ignored in the current study.

Finally, reactor pool simulation was performed at 2 MW power at 0.25 m/s velocity with a reactor core modeled as porous media. It was observed to operate at a safe

temperature limit. The study concludes about the application of porous media modeling as a candidate for nuclear research reactor thermal-hydraulics simulation alongside realistic modeling.

ACKNOWLEDGEMENTS

This work was supported in part by the Kummer Institute at Missouri Science and Technology through the Kummer I&E Doctoral Fellowship bestowed to the first author. The authors also extend their appreciation to the Missouri University of Science and Technology for granting access to high-performance computation and software.

REFERENCES

Ahmed, F., Ara, N., Deshpande, V., Mollah, A. S., & Bhowmik, P. K. (2021). CFD validation with optimized mesh using benchmarking data of pebble-bed high-temperature reactor. Progress in Nuclear Energy, 134. https://doi.org/10.1016/j.pnucene.2021.103653

Akyurek, T., & Usman, S. (2015). Spent fuel interrogation using delayed fast neutron spectrum at Missouri University of Science and Technology Reactor. Progress in Nuclear Energy, 85, 525–540. https://doi.org/10.1016/j.pnucene.2015.07.021

Alhuzaymi, T. M., ALQahtani, M. M., Aljuwaya, T. M., & Alajo, A. B. (2023). MCNP and CFD Modeling for Potential High-Power Configuration of Missouri S&T Reactor. Processes, 11(4), 1044. https://doi.org/10.3390/pr11041044

Bae, J., & Bean, R. S. (2022). Investigation of Thermohydraulic Limits on Maximum Reactor Power in LEU Plate–Fueled, Pool-Type Research Reactor. Nuclear Science and Engineering, 196(10), 1224–1235. https://doi.org/10.1080/00295639.2022.2055700

Bhowmik, P. K., & Schlegel, J. P. (2023). Multicomponent gas mixture parametric CFD study of condensation heat transfer in small modular reactor system safety. Experimental and Computational Multiphase Flow, 5(1), 15–28. https://doi.org/10.1007/s42757-022-0136-8

Bonzer, W., & Carroll, C. (2008). Safety analysis report for the missouri university of science and technology reactor-revision 2.

Cameron, R., & Horlock, K. (2001). The Replacement Research Reactor.

Carmack, J., Goldner, F., Bragg-Sitton, S. M., & Snead, L. L. (2013). Overview of the U.S. DOE Accident Tolerant Fuel Development Program Top Fuel 2013 Overview of the U.S. DOE Accident Tolerant Fuel Development Program.

Castano Giraldo, C. H., Liu, X., Alajo, A., Castano, C., Kumar, A., Liu, X., & Alajo, A. (2013). Active Heat Removal System for Continuous Operation of the Missouri S&T Reactor. Transactions of the American Nuclear Society, 109. https://www.researchgate.net/publication/286955049

Freile, R., Tano, M., Balestra, P., Schunert, S., & Kimber, M. (2021). Improved natural convection heat transfer correlations for reactor cavity cooling systems of high-temperature gas-cooled reactors: From computational fluid dynamics to Pronghorn. Annals of Nuclear Energy, 163. https://doi.org/10.1016/j.anucene.2021.108547

Ge, J., Wang, C., Xiao, Y., Tian, W., Qiu, S., Su, G. H., Zhang, D., & Wu, Y. (2016). Thermal-hydraulic analysis of a fluoride-salt-cooled pebble-bed reactor with CFD methodology. Progress in Nuclear Energy, 91, 83–96. https://doi.org/10.1016/j.pnucene.2016.01.011

Hedayat, A., & Davari, A. (2022). Feasibility study to increase the reactor power at natural convection mode in Tehran Research Reactor (TRR) through a hybrid thermal-hydraulic simulation and analysis using the RELAP5 code and Computational Fluid Dynamic (CFD) modeling by ANSYS-FLUENT. Progress in Nuclear Energy, 150. https://doi.org/10.1016/j.pnucene.2022.104285

Jareteg, K., Vinai, P., & Demazière, C. (2014). Fine-mesh deterministic modeling of PWR fuel assemblies: Proof-of-principle of coupled neutronic/thermal-hydraulic calculations. Annals of Nuclear Energy, 68, 247–256. https://doi.org/10.1016/j.anucene.2013.12.019

Ju, H., Wang, M., Chen, C., Zhao, X., Zhao, M., Tian, W., Su, G. H., & Qiu, S. (2019). Numerical study on the turbulent mixing in channel with Large Eddy Simulation (LES) using spectral element method. Nuclear Engineering and Design, 348, 169–176. https://doi.org/10.1016/j.nucengdes.2019.04.017

Mahaffy, J. , Chung, B. , Song, C. , Dubois, F. , Graffard, E. , Ducros, F. , Heitsch, M. , Scheuerer, M. , Henriksson, M. , & Komen, E. ,. (2007). Best practice guidelines for the use of CFD in nuclear reactor safety applications. Technical Report, Organization for Economic Co-Operation and Development, IAEA 44(1) (13(1)).

Menter, F., Sechner, R., & Matyushenko, A. (2021). Best Practice: RANS Turbulence Modeling in Ansys CFD.

Mira, M., El Hajjaji, O., El Bardouni, T., Al-Zain, J., & Oulad-Belayachi, S. (2023). Innovative and advanced fuel based on nuclear waste transuranic nuclides: An alternative fuel for TRIGA Mark II research reactor. Annals of Nuclear Energy, 192. https://doi.org/10.1016/j.anucene.2023.109998

Morselli, L., Donzella, A., Arzenton, A., Asti, M., Bortolussi, S., Corradetti, S., D'Agostino, G., Di Luzio, M., Ferrari, M., Gandini, A., Lunardon, M., Villa, V., Salvini, A., Zangrando, L., Zenoni, A., & Andrighetto, A. (2023). Production and characterization of 111Ag radioisotope for medical use in a TRIGA Mark II nuclear research reactor. Applied Radiation and Isotopes, 197. https://doi.org/10.1016/j.apradiso.2023.110798

Ricciardi, G., Bellizzi, S., Collard, B., & Cochelin, B. (2009). Modelling Pressurized Water Reactor cores in terms of porous media. Journal of Fluids and Structures, 25(1), 112–133. https://doi.org/10.1016/j.jfluidstructs.2008.04.002

Richardson, B., Castano, C. H., King, J., Alajo, A., & Usman, S. (2012). Modeling and validation of approach to criticality and axial flux profile experiments at the Missouri S&T Reactor (MSTR). Nuclear Engineering and Design, 245, 55–61. https://doi.org/10.1016/j.nucengdes.2012.01.023

Sipaun, S., & Usman, S. (2015). Prediction of Missouri S&T Reactor's natural convection with porous media approximation. Nuclear Engineering and Design, 285, 241–248. https://doi.org/10.1016/j.nucengdes.2015.01.001

Sosnowski, M., Krzywanski, J., & Gnatowska, R. (n.d.). Polyhedral meshing as an innovative approach to computational domain discretization of a cyclone in a fluidized bed CLC unit. https://doi.org/10.1051/4

Spalart, P. R. (2000). Strategies for turbulence modelling and simulations. International Journal of Heat and Fluid Flow, 252–263. www.elsevier.com/locate/ijh

Steiner, T. R., Hutchins, E. N., & Howard, R. H. (2022). Steady-State In-Pile Nuclear Thermal Propulsion Experimental Testbed Initial Demonstration at The Ohio State University Research Reactor. Nuclear Technology, 208(1), 100–114. https://doi.org/10.1080/00295450.2021.1879582

Terrani, K. A. (2018). Accident tolerant fuel cladding development: Promise, status, and challenges. In Journal of Nuclear Materials (Vol. 501, pp. 13–30). Elsevier B.V. https://doi.org/10.1016/j.jnucmat.2017.12.043

Tusar, M., Ahmed, K., Bhuiya, M., Bhowmik, P., Rasul, M., & Ashwath, N. (2019). CFD study of heat transfer enhancement and fluid flow characteristics of laminar flow through tube with helical screw tape insert. Energy Procedia, 160, 699–706. https://doi.org/10.1016/j.egypro.2019.02.190

Tusar, M. H., Bhowmik, P. K., Salam, B., Uddin Ahamed, J., & Kim, J. K. (2021). Convective heat transfer and friction factor characteristics of helical strip inserted annuli at turbulent flow. International Journal of Heat and Mass Transfer, 176, 121422. https://doi.org/10.1016/j.ijheatmasstransfer.2021.121422

Tusar, M., Noman, A., Islam, M., Yarlagadda, P., & Salam, B. (2019). CFD study of heat transfer enhancement and fluid flow characteristics of turbulent flow through tube with twisted tape inserts. Energy Procedia, 160(2018), 715–722. https://doi.org/10.1016/j.egypro.2019.02.188

Umar, E., Rohim Iso, A., Aziz, A., & Ilmar Ramadhan, A. (2023). Theoretical and experimental investigation of the thermal–hydraulic parameters of the Bandung TRIGA research reactor. Annals of Nuclear Energy, 193. https://doi.org/10.1016/j.anucene.2023.110020

Wakabayashi, G., Yamada, T., Endo, T., & Pyeon, C. H. (2023). Test and Research Reactors in Japan. In G. Wakabayashi, T. Yamada, T. Endo, & C. H. Pyeon (Eds.), Introduction to Nuclear Reactor Experiments (pp. 125–136). Springer Nature Singapore. https://doi.org/10.1007/978-981-19-6589-0_4

Wang, Y., Wang, M., Ju, H., Zhao, M., Zhang, D., Tian, W., Liu, T., Qiu, S., & Su, G. H. (2020). CFD simulation of flow and heat transfer characteristics in a 5×5 fuel rod bundles with spacer grids of advanced PWR. Nuclear Engineering and Technology, 52(7), 1386–1395. https://doi.org/10.1016/j.net.2019.12.012

Wu, C. Y., Ferng, Y. M., Chieng, C. C., & Liu, C. C. (2010). Investigating the advantages and disadvantages of realistic approach and porous approach for closely packed pebbles in CFD simulation. Nuclear Engineering and Design, 240(5), 1151–1159. https://doi.org/10.1016/j.nucengdes.2010.01.015

Yan, B. H., Gu, H. Y., & Yu, L. (2011). Numerical research of turbulent heat transfer in rectangular channels in ocean environment. Heat and Mass Transfer, 47(7), 821–831. https://doi.org/10.1007/s00231-011-0770-3

Yan, Y. (2011). Development of a coupled cfd-system-code capability (with a modified porous media model) and its applications to simulate current and next generation reactors.

Yasuda, Y., Nabeshima, F., Horiuchi, K., & Nagai, H. (2022). Visualization of the working fluid in a flat-plate pulsating heat pipe by neutron radiography. International Journal of Heat and Mass Transfer, 185. https://doi.org/10.1016/j.ijheatmasstransfer.2021.122336

Yun, D., Lu, C., Zhou, Z., Wu, Y., Liu, W., Guo, S., Shi, T., & Stubbins, J. F. (2021). Current state and prospect on the development of advanced nuclear fuel system materials: A review. In Materials Reports: Energy (Vol. 1, Issue 1). KeAi Communications Co. https://doi.org/10.1016/j.matre.2021.01.002

Zhang, K. (2020). The multiscale thermal-hydraulic simulation for nuclear reactors: A classification of the coupling approaches and a review of the coupled codes. In International Journal of Energy Research (Vol. 44, Issue 5, pp. 3295–3315). John Wiley and Sons Ltd. https://doi.org/10.1002/er.5111

Zou, L., Peterson, J. W., Martineau, R. C., Slaybaugh, R. N., & Novak, A. J. (2018). Pronghorn: A Porous Media Thermal-Hydraulics Core Simulator and its Validation with the SANA Experiments. http://www.inl.gov

II. IMPACT OF SURFACE AND PHYSICAL PROPERTY ON MULTIPHASE FLOW IN SEALED VESSEL: LIQUID DROPDOWN PERFORMANCE

Mehedi Hasan Tusar[1], Palash K. Bhowmik[1,2], Kazuma Kobayashi[3], Syed Alam[3], Shoaib Usman[1]*

[1] Department of Nuclear Engineering and Radiation Science, Missouri University of Science and Technology, Rolla, MO 65409, USA

[2] Department of Irradiation Experiment and Thermal-hydraulics Analysis, Idaho National Laboratory, Idaho Falls, ID 83415, USA

[3] Department of Nuclear, Plasma & Radiological Engineering, University of Illinois at Urbana–Champaign, Urbana, IL 61801, USA

ABSTRACT

This study explores multi-phase (i.e., liquid-gas) and multi-fluid (i.e., air-water, and water-silicone oil) flow-pattern and flow-blockage physics phenomena for wall wettability conditions ranging from superhydrophilic to superhydrophobic cases in sealed vessels utilizing computational fluid dynamics (CFD) simulation tools and volume-of-fluid (VOF) method with sharp interface modeling. Detailed modeling and simulation (M&S) of such physics phenomena—in which liquid (e.g., water) stands over top of gas (e.g., air or steam) in a closed channel and exhibited flow blockage, flow reversal related challenges—are pivotal for design, analysis, and qualification of component-level (e.g., heat pipes, heat exchangers) to system-level (e.g., emergency core cooling systems in nuclear reactors) heating and cooling industrial applications. Results show that, these physics phenomena are dependent on factors like contact angle (CA), channel diameter, gravity, and viscosity which impact the flow behavior in an adiabatic, and closed environment. Key observations include the role of CA (for 10, 50-, 90-, 130-, and 170-degree) in dropdown time: (a) a

quicker dropdown for higher wettability surfaces (CA < 90 degrees); and (b) a slower dropdown for normal (CA = 90 degrees) and lower wettability surfaces (CA > 90 degrees). Other important observations are: (a) channel diameter (for 3, 10, and 100 mm) emerges as a crucial factor, a completely blocking flow case; (b) gravity variations introduce further complexities, leading to more unpredictable and unsteady flows under reduced gravity conditions. These findings, observations, and insights, including quantitative, qualitative and nondimensional analysis supports design optimization, enhanced components-to-system level heat-transfer performance for relevant engineering applications.

Keywords. Rayleigh-Taylor instability, Heat pipes, Wettability, Computational fluid dynamics, Volume of fluid

1. INTRODUCTION

Flow in vertically sealed tubes and capillaries have engineering applications in nuclear reactor systems such as reactor core flooding, micro reactors, and heat pipes (Jose & Kumar Hotta, 2023; Testoni et al., 2021). Ensuring continuous flow and preventing flow blockage is desired in these engineering systems. During a loss of coolant accident (LOCA), the cooling fluid in the reactor is depleted, causing the fuel rods to overheat, generating a significant volume of steam. To mitigate this, water is injected into the reactor at various pressures known as reactor core flooding (Murao et al., 1982). There is a chance of flow blockage during flooding. The Rayleigh-Taylor (RT) instability is a fluid-dynamical phenomenon that can help prevent flow blockage. It arises when a fluid with a higher density is situated above a fluid with a lower density. This configuration leads to complex flow patterns and structures as the heavier fluid penetrates the lighter one due to

gravitational forces (Gallaire & Brun, 2017). The perturbation growth, shape of the liquid dropping depends on Atwood number (Tang et al., 2021). When the water is injected from above, the setup for RT instability is inherently created as the denser water overlays the lighter steam. This results in an unstable interface between steam and water, and the water descends through the steam in finger-like structures or plumes, with some of the water streaming down the vessel walls. RT instability can, under certain conditions, enhance the cooling performance by facilitating the mixing of water with steam. However, it may also impede the even and rapid distribution of water within the reactor vessel, which is particularly problematic if large steam bubbles are entrapped within the water, consequently reducing the effective cooling of the fuel rods. The dynamics of the flow in such scenarios is complex and necessitates rigorous experimental and computational analysis for verification and validation prior to integration into reactor designs (Li et al., 2021).

Microreactors, with their high surface-area to volume ratio, enhance heat transfer and use coatings to adjust wettability, driving interest in heat pipes for thermal management in energy and propulsion systems (Maresz et al., 2020; Szymańska et al., 2021). These monolithic heat pipe based microreactors exhibit thermal conductivities between 5,000 to 200,000 W/m-K, significantly outperforming traditional materials like aluminum, copper, and diamond. Their high performance is achieved through thermal conduction and phase transitions of the working fluid, notably water, which enables substantial heat transfer with minimal temperature differences. Specifically, heat pipes with lithium can transfer heat at rates up to 23,000 W/cm² (Grabaskas, 2019). In the context of gravitational or thermosyphon heat pipes, heat is supplied to the liquid at the bottom, which upon

vaporization, rises and releases heat during condensation at the top. This configuration operates passively, without the need for external power sources or moving parts, rendering it especially viable for space applications (Wang et al., 2020). However, in such systems, there is an inherent risk of the condensed liquid impeding the flow within the capillary channels due to the interplay of surface tension and viscosity. This can lead to system failure. Thus, conducting a thorough examination of how wettability, surface tension, gravity, and viscosity influence flow behavior is crucial for the optimization and robust design of such systems.

Several works have been done in the past years to improve flow performance and prevent blockage. Taylor bubble flow is a common phenomenon on heat pipes. The steady unidirectional Taylor bubble flow is well-understood in terms of parameters such as liquid film thickness, bubble velocity, and pressure drop. However, the oscillating Taylor bubble flow, which is prevalent in pulsating heat pipes (PHP), is not yet well comprehended. This incomplete understanding of pulsating heat pipes poses challenges in analyzing the behavior of systems employing them, especially as the oscillating Taylor bubble flow complicates the scenario (Khandekar et al., 2010). Angeli and Gavriilidis (Angeli & Gavriilidis, 2008) highlighted constraints on Taylor bubble flow in very small channels and the dominance of surface tension in channels of 1 and 2 mm. Additionally, the phenomena of condensation, even at the evaporator in microgravity conditions of International Space Station, as observed by Kundan et al. (Kundan et al., 2015, 2017), raise concerns regarding the flow stability in such systems. If the system configuration is not equipped to maintain flow, there is a substantial risk of flow entrainment and subsequent system failure. Given the challenges with PHPs, it is imperative to develop designs that

mitigate the risk of flow blockage. Interestingly, enhancing the RT instability can be beneficial because it may reduce the likelihood of flow blockage. It is essential to recognize that RT instability in sealed vessels or capillaries is influenced by various factors, such as fluid temperature, surface tension, gravity, viscosity, wettability, channel diameter, and density differences (Awati et al., 2019; Eggers & Villermaux, 2008; D. L. Youngs, 2013; Zanella et al., 2021a). Swelling of claddings on flat plate nuclear fuels is concern as it reduces the flow path, increasing the chance of flow blockage. For rod bundle type fuel, flow bypass happens in case of complete or partially blocked channels (Oliveira et al., 2020). Experimental and numerical studies on narrow rectangular channels show that spherical crown protrusions due to swelling affect convective heat transfer, with streamwise alignments worsening heat transfer by over 20% (Xu et al., 2022). As experimental techniques are costly, time-consuming significant amount of the thermal hydraulic study of capillary and reactors were performed using computational fluid dynamics (CFD). Volume Of Fluid (VOF) and Lee phase-change models were utilized to analyze PHPs with 7, 16, and 23 turns. These models were validated against experimental data and a semi-empirical correlation to investigate flow instability and heat transfer within PHPs (Mucci et al., 2021). Another study used homogeneous multiphase model with source terms inspired by the Lee phase change model for evaporation and condensation processes to simulate the steam/water two-phase flow and heat transfer in heat pipes (Höhne, 2022). Dinesh and Narayanan (Dinesh & Narayanan, 2021a) took a closer look at RT instability by exploring the effects of horizontal boundaries on wave behavior in viscoelastic fluids under RT instability. They reported different wave characteristics based on whether the horizontal boundary is bounded or unbounded. Khan and Shah (Khan & Shah, 2019)

employed the diffuse interface model with the Boussinesq approximation for density variation. Wettability can be controlled in simulations by contact-angle (CA) implementation (Huhtamäki et al., 2018). Hassan et al. (Ul Hassan et al., 2021) used electric field potential and wettability to control the penetration depth of liquid inside capillary. They performed numerical analysis that agreed well with the experimental study. However, there is a paucity of literature on the impact of varying surface wettability on RT instability and flow entrainment. This presents an area ripe for further investigation.

Building on prior discussions regarding the flow blockage in two-phase flow systems, this study investigates the combined effects of CA, channel diameter, gravity, and viscosity on the dropdown performance of a denser liquid over a lighter fluid. Using a three-dimensional CFD approach with the VOF method, the stability of the gas-liquid interface is examined under different wettability conditions, represented by CAs ranging from superhydrophilic to superhydrophobic. The primary objective is to discern how these parameters collectively govern the interface stability, and to identify conditions that may lead to flow blockage. This includes nondimensional analysis of different flow conditions to check the effect of inertia, gravitational, surface tension, and viscous force. The flow visualization is done for understanding patterns and quantitative evaluation of dropdown times.

2. METHODOLOGY AND SIMULATION PROCEDURE

2.1. METHODOLOGY

We had used three different geometries of 3-, 10- and 100-mm diameter. All the channels were sealed in the top and bottom. The selected diameters cover the range from capillary to tube for water flow (Liu et al., 2005). All the channel configurations had a total length of 400 mm. The upper half of this channel was filled with water whereas the lower half of the channel was filled with air. We tested five CA of 10, 50, 90, 130 and 170 degrees to check how wettability conditions as superhydrophilic, hydrophilic, normal, hydrophobic, and superhydrophobic walls affect dropdown performance, as shown in Figure 1. The working fluids are air-water systems in most cases whereas a silicone oil-air system was also investigated to check the effect of viscosity. Their properties are listed on Table 1. The gravitational acceleration values of 9.81 and 3.72 ms^{-2} were used to check the effect of gravity on flow nature and dropdown performance. ANSYS FLUENT, a commercial software package, was used to perform the VOF simulation.

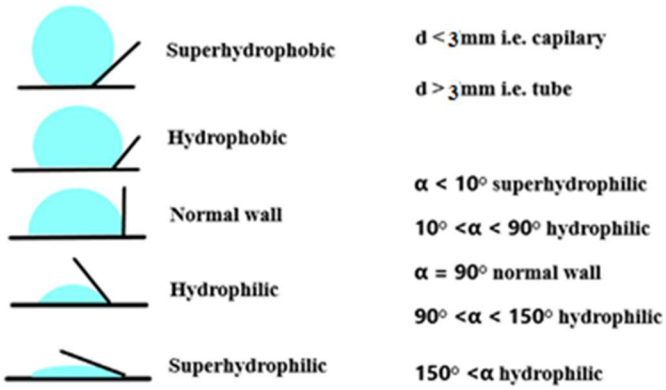

Figure 1. Different wettability of walls in capillaries and tubes.

Table 1. Physicochemical properties of working fluids tested in the study.

Properties	Air	Water	Silicone oil
Density, ρ (Kg/m$^{3)}$	1.225	998.2	950
Specific heat, C_p (J/ Kg. K)	1006	4182	1300
Dynamic viscosity, μ (Kg/ m. s)	1.7894 x 10^{-5}	0.001003	19 x 10^{-3}
Thermal conductivity, k (W/ m. K)	0.0242	0.6	0.2
Surface tension, σ (N. m)	- -	0.072 (air-water)	0.04 (air-silicone oil)

2.2. DOMAIN DISCRETIZATION AND BOUNDARY CONDITIONS

We have tested the fluid domain only as solid domain properties were included in the wall. The fluid domain was created in SolidWorks, later the Computer-Aided Design file was imported into Fluent workbench as a stereolithographic (STL) file. The domain discretization was performed in ICEM CFD. A combination of tetrahedral and prism mesh was used for initial discretization. Lower mesh size increases accuracy of computation, and it also increases computation time and resource. Therefore, we used smaller and larger mesh size for capillary and tube, respectively, for optimum use of resource considering accuracy. We have used a mesh maximum face size of 0.2-, 1.5-, and 3-mm for 3-, 10-, and 100-mm diameter channels, respectively. The flow variables change abruptly near the wall region; this is especially important when dealing with viscous flows. The boundary layer, where velocity changes from zero at the wall to the free stream value needs remarkably high resolution for increased accuracy and solution convergence. Therefore, we have used inflation layers in the wall region which are smaller-size meshes than the free-stream region. Five inflation layers were used with a 1.2 progression ratio of inflation-

layer heights. We converted the initial combination of tetrahedral and prism mesh into polyhedral mesh because it provides a lower amount of mesh-element flexibility in conforming to complex geometries, reduced computation time, and good accuracy (Sosnowski et al., n.d.). A partial view of the final mesh is shown in Figure 2. The fluid domain was isolated from the surroundings; thus, there was no heat or energy transfer across the system boundary. This isothermal adiabatic system was also closed by solid walls maintained at zero heat flux. The solid walls had controllable wettability, which is controlled by CA. No slip-momentum boundary condition was implemented at the fluid/solid interface as used by (Hassan, 2021) for different wettability surfaces. The air/water interface changes its position every time step. Mesh refinement in the newest interface positions and coarsening in the previous interface position will reduce computational time and provide better accuracy. Therefore, adaptive mesh refinement was used in this study, which changes the mesh every time step. Mesh refinement was performed in the cells, which had a concentration gradient higher than 0.06 and coarsened below that value.

2.3. GOVERNING EQUATIONS AND SOLUTION PROCEDURE

The solution was transient in nature. Gravity was the driving force for liquids under consideration. Two immiscible fluids that maintain two separate phases are ideal candidates for VOF modeling (Mulbah et al., 2022). Water was the primary phase, and air was the secondary phase in our current study. Pressure-based solver was used. The total summation of all volume fraction, α, for fluids in every discretized cell is equal to one. For qth fluid $\alpha_q = 0$, when the cell is empty, $\alpha_q = 1$ means the cell is full and $0 < \alpha_q < 1$ means

the cell contains the interface between the qth fluid and other fluid. The continuity equation was used for interface tracking between the phases, as shown in Equation 1.

$$\frac{1}{\rho_q}\left[\frac{\partial}{\partial t}\left(\alpha_q \rho_q\right) + \nabla \cdot \left(\alpha_q \rho_q \vec{v}_q\right) = S_{\alpha_q} + \sum_{p=1}^{n} \left(\dot{m}_{pq} - \dot{m}_{qp}\right)\right] \quad (1)$$

Where ρ, $\vec{v}$ are density, velocity and $\dot{m}_{pq}$, $\dot{m}_{qp}$ are the mass transfer from phase p to q and vice versa. There are no source terms and mass transfer between air and water phase. So, Equation 1 becomes simplified form of Equation 2.

$$\frac{\partial}{\partial t}\left(\alpha_q \rho_q\right) + \nabla \cdot \left(\alpha_q \rho_q \vec{v}_q\right) = 0 \quad (2)$$

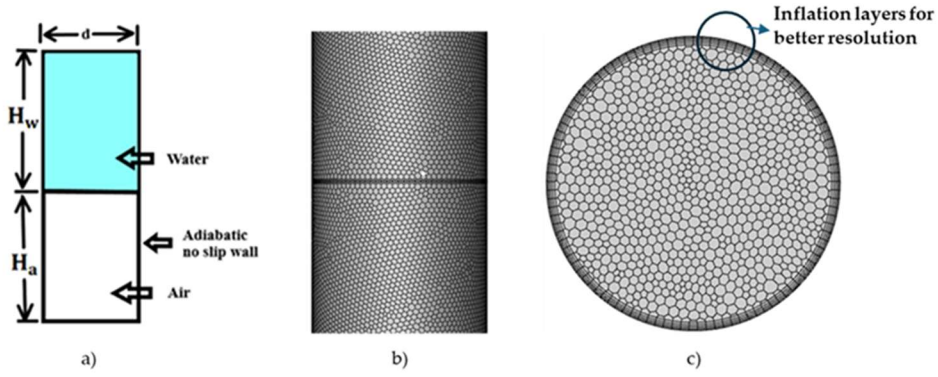

Figure 2. a) Schematic for flow domain; b) partial view of the air/water interface meshing; c) cross section view of the fluid-domain meshing.

The explicit scheme of Equation 3 was used for time discretization. Face fluxes were interpolated using geometric reconstruction (Youngs, 1982). Quadratic upstream interpolation for convective kinematics (QUICK) scheme (Leonard, 1979) was used for unsteady convective-diffusion equation solution. QUICK is widely used in complex flows (Tusar et al., 2021). Where n, n+1 is the previous and current time step. $\alpha_{q,f}$ is the face

volume fraction from QUICK scheme, V is volume of cell and U_f is volume flux through the face based on the normal velocity.

$$\frac{\alpha_q^{n+1}\rho_q^{n+1}-\alpha_q^n\rho_q^n}{\Delta t}V + \sum_f \left(\rho_q U_f^n \alpha_{q,f}^n\right) = \left[\sum_{p=1}^n \left(\dot{m}_{\mathrm{pq}} - \dot{m}_{\mathrm{qp}}\right) + S_{\alpha_\mathrm{q}}\right]V \quad (3)$$

Any material properties, X, that appear in the continuity equation were calculated using Equation 4. SST-kω turbulence model developed by Menter (Menter, 1994) was used for viscosity modeling as it is used in heat pipe, capillary flow and VOF (Höhne, 2022).

$$X = \alpha_2 X_2 + (1-\alpha_2)X_1 \quad (4)$$

The momentum equation described in Equation 5 was solved throughout the domain, and velocity information was shared between the phases. Here $\vec{v}, \rho\vec{g}, \vec{F}$ are velocity, gravity force and external body forces, respectively. Proper capture of surface tension phenomena is necessary for interface tracking and external body-force measurement in the momentum equation. It was modeled as continuum surface force using the methodology of Brackbill et al. (Brackbill et al., 1992) using Equations 6 and 7. Here p_1, p_2 and R_1, R_2 are the pressure and radius of surface curvature in the water and air phase, respectively. F and k are the forces at the surface and convergence, respectively. The effect of CA, θ_w in the surface tension was included, using Equation 8 from the same literature, where $\hat{n}, \hat{n}_w,$ and $\hat{t}_w$ are the resultant unit vector, unit vectors normal and tangential to wall, respectively.

$$\frac{\partial}{\partial t}(\rho\vec{v}) + \nabla\cdot(\rho\vec{v}\vec{v}) = -\nabla p + \nabla\cdot[\mu(\nabla\vec{v} + \nabla\vec{v}^T)] + \rho\vec{g} + \vec{F} \quad (5)$$

$$p_2 - p_1 = \sigma\left(\frac{1}{R_1} + \frac{1}{R_2}\right) \quad (6)$$

$$F = \sigma_{ij}\frac{\rho\kappa_i\nabla\alpha_i}{\frac{1}{2}(\rho_i+\rho_j)} \quad (7)$$

$$\hat{n} = \hat{n}_w \cos\theta_w + \hat{t}_w \sin\theta_w \quad (8)$$

The solution was performed explicitly. Therefore, Courant number, C in a multidimensional grid, as described in Equation 9, was kept <1 where $U_i, \Delta t,$ and Δh are flow velocity, time step, and mesh size, respectively. The patching method was used to initialize water and air volume in the upper and lower half of the geometry. Pressure-implicit with splitting of operators was used as the pressure-velocity coupling technique. Intel Core i9-10900 Central Processing Unit with 2.8 GHz clock speed and 20 logical processors were used for parallel processing in this study. The High-Performance Computing Facility through cloud was also used for computation.

$$C = \sum_i \frac{U_i \, \Delta t}{\Delta h} \tag{9}$$

2.4. NONDIMENSIONAL ANALYSIS

Equation 10, the Weber number (We), quantifies the dominance of fluid inertia relative to the force of surface tension. Equation 11, the Bond number (Bo), evaluates the significance of gravitational forces in contrast to surface tension forces. Equation 12, the Ohnesorge number (Oh), measures the impact of viscous forces in comparison to both inertial and surface tension forces. For Equations 10 through 13, the characteristic length used is the diameter, d of the channel.

$$We = \frac{\rho V^2 d}{\sigma} \tag{10}$$

$$Bo = \frac{\Delta \rho g d^2}{\sigma} \tag{11}$$

$$Oh = \frac{\mu}{\sqrt{\rho \sigma d}} \tag{12}$$

3. RESULTS AND DISCUSSIONS

3.1. GRID SENSITIVITY CHECK AND VALIDATION

We tested three different meshes of maximum face sizes of 1-, 1.5-, and 2.5 mm in a 90-degree CA wall for a 10-mm-diameter sealed vessel. Grid sensitivity was tested in terms of the dropdown time of the total water fraction. Table 2 shows the dropdown time for different mesh sizes. We finally selected a 1.5-mm mesh size because it gives a lower amount of mesh, yet good result. Similarly, 0.2-, and 3-mm mesh sizes were chosen for 3-mm and 100-mm sealed vessels. Accurate prediction of the RT instability and other flow behaviors in two-phase flow depends on proper capturing of interfaces. Therefore, we validated our simulation method with the study of Liu et al. (Liu et al., 2005). This current simulation method was used to simulate the flow regime in d = 3.02 mm capillary of L = 1.4 m in the vertical upward flow of an air-water mixture. A T-connection was used for the air and water inlet. The velocity of air and water flow were 0.1 m/s and 0.01 m/s, respectively. The flow-regime map at this flow condition suggests it to be a Taylor flow region, which was also observed in our current study, as shown in Figure 3. Every air-entrapped region was followed by a liquid slug where one consecutive air bubble and liquid slug forms the unit cell. We determined the theoretical-unit cell length using Equation 13 and compared it with the measurements performed in the current study. In this study, L_{uc}, V_b, and f_b represent the length of the unit cell, bubble-rise velocity, and bubble frequency, respectively. In our simulations, V_b, f_b, and L_{uc} were measured using ImageJ software. Two different images at t = 5.75 and 6 s were used for this analysis. Theoretical and measured data are represented in Table 3 which shows a close match between them.

$$L_{uc} = \frac{V_b}{f_b} \tag{13}$$

Table 2. Grid sensitivity check in terms of drop-down time.

Mesh size	Dropping time
2.5 mm, 172102 cells	2.61 s
1.5 mm, 481707 cells	2.4 s
1 mm, 1028033 cells	2.42 s

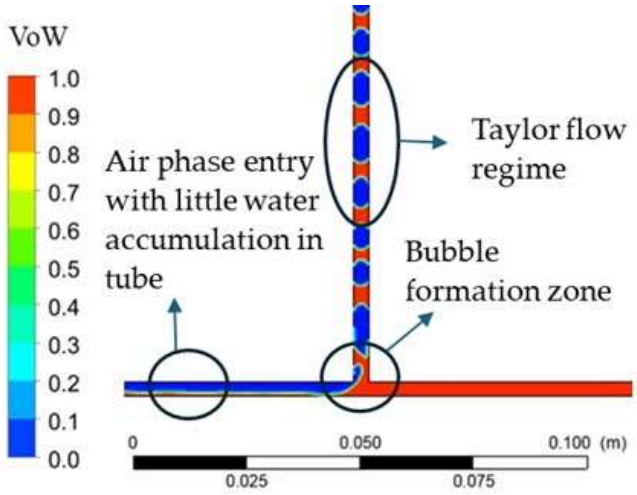

Figure 3. Current CFD study validation with Liu et al. (Liu et al., 2005) in Taylor flow regime.

Table 3. Comparison of theoretical and actual unit cell length.

Sample no.	1st	2nd	3rd	4th
Luc, theory (mm)	9.25	9.25	9.25	9.5
Luc, actual (mm)	10	9	11	12

3.2. ROLE OF CONTACT ANGLE

All the simulations were performed in zero-gauge pressure. Figure 4 represents the pressure contour from beginning to finishing of the dropdown time. Initially, the water-column height was 20 cm above air column of 20 cm. The fluid domain was initialized with zero-gauge pressure; therefore, the air column had 0 Pa pressure at t = 0 s. The static pressure was -2014 Pa at the top of the water column. which gradually increased to 0 Pa. The negative sign indicates that higher-density fluid is on top of a lighter fluid. Confusion should be avoided by considering it as vacuum pressure. The gravitational force pushes the water downwards and changes the pressure field. When the water column reached the bottom part of the container, static pressure reached 2014 Pa, validating that the water column was below the air column. The static pressure contours were checked for sealed vessels of contact angles of 10, 90 and 170 degrees, representing superhydrophilic, normal, and superhydrophobic walls, respectively. The diameter of the vessels was 100 mm. It was observed that dynamic pressure had a minor impact on the static pressure as the flow velocity was comparatively small. Similarly, static pressure contours had small dependency on flow patterns on different types of walls under current investigation. The dropdown time for different types of containers was different, but the pressure contour pattern was similar in all the cases.

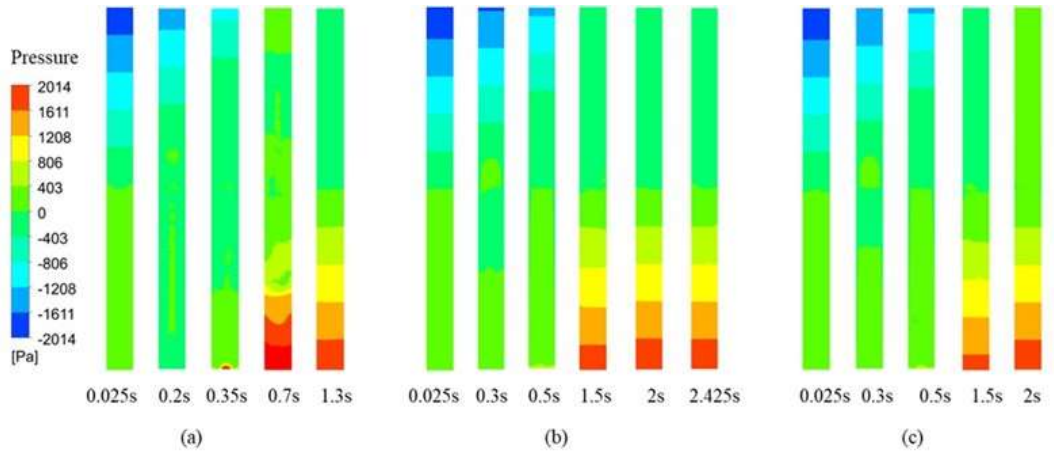

Figure 4. Pressure contour in the midplane for d= 100 mm and a) CA 10 degrees, b) CA 90 degrees, and C) CA 170 degrees.

We checked five distinct types of vessels as superhydrophilic, hydrophilic, normal, hydrophobic and superhydrophobic walls of 10, 50-, 90-, 130- and 170-degrees CA, respectively, for d = 100 mm. Figure 5 represents dropdown time for total volume of water for the investigated vessels. It was observed that dropdown time follows the trend as superhydrophilic < hydrophilic < superhydrophobic < hydrophobic < normal. Total dropdown time for superhydrophilic was 1.3 s whereas it was 2 and 2.42 s for superhydrophobic and normal walls, respectively. A proper understanding of this observation can be realized from Figure 6. The flow patterns were different for superhydrophilic sealed vessels than the normal and superhydrophobic ones. The superhydrophilic surface has an extremely high affinity for water. This strong interaction of surface wall with water makes water drop down difficult through-vertical surfaces. It is observed, from Figure 6a, that water was stagnant with the surface at t = 0.025 s. There were small perturbations present in the beginning, which amplified with time as interfacial and gravitational forces were present. The gravity force generates instability, which makes the water drop down whereas viscous and surface-tension forces try to maintain the

stability of the air-water interface. The amplified perturbation produced finger-like projections of liquid columns, which merged into one single free-falling vertical water column as time progressed. This vertical free-falling column had a higher flow rate and, thus, the lowest drop-down time. The higher flow rates of free fall produced splashes of liquids and turbulent mixing of water in the presence of trapped air bubbles. The bubbles rise in the liquid column due to buoyancy, and both phases were separated at t = 1.3 s. The attraction for water was moderate for normal walls in Figure 6b. Therefore, water poured down via the contact with the container wall. A ring of thick water column was present at the forefront of drooping liquid. A similar flow pattern was also observed for superhydrophobic walls, as depicted in Figure 6c. However, the thick ring was absent in the forefront for this flow. Therefore, it is realized that attraction force is lowest between the surface and water, so the flow was faster in this wall than the normal wall. It requires t = 2 s for a superhydrophobic wall whereas it takes t = 2.42 s for normal walls. Similar results was also observed by (Zanella et al., 2021b) in their simulation of multiphase corium. The thin heavier liquid metal layer residing above molten liquid pool produced finger-like protrusions by RT instability, which later formed droplets by Rayleigh-Plateau instability. In the nondimensional analysis depicted in Figure 5, which employs the We, it is noted that normal walls exhibit the lowest inertia during the descent of droplets. This is succeeded by superhydrophobic walls when water descends along the wall. The We reaches its maximum for superhydrophobic walls during the free fall of water through interface breakup, indicating the greatest dominance of inertia over surface tension force, and consequently, resulting in the quickest descent of the flow.

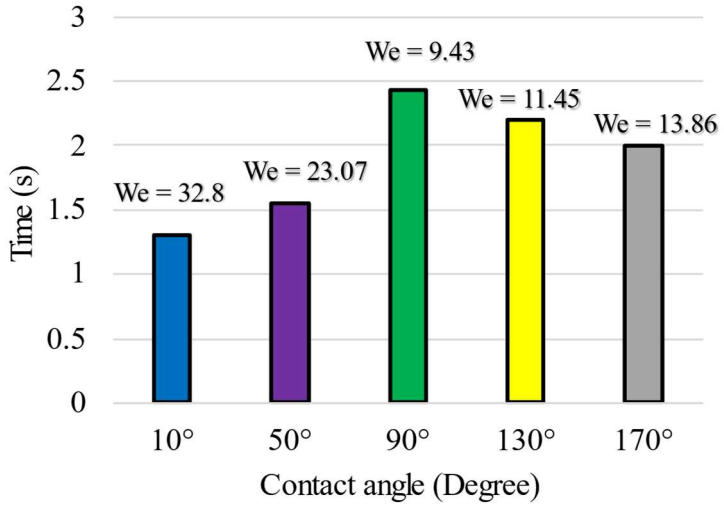

Figure 5. CA vs dropdown time at d= 100 mm.

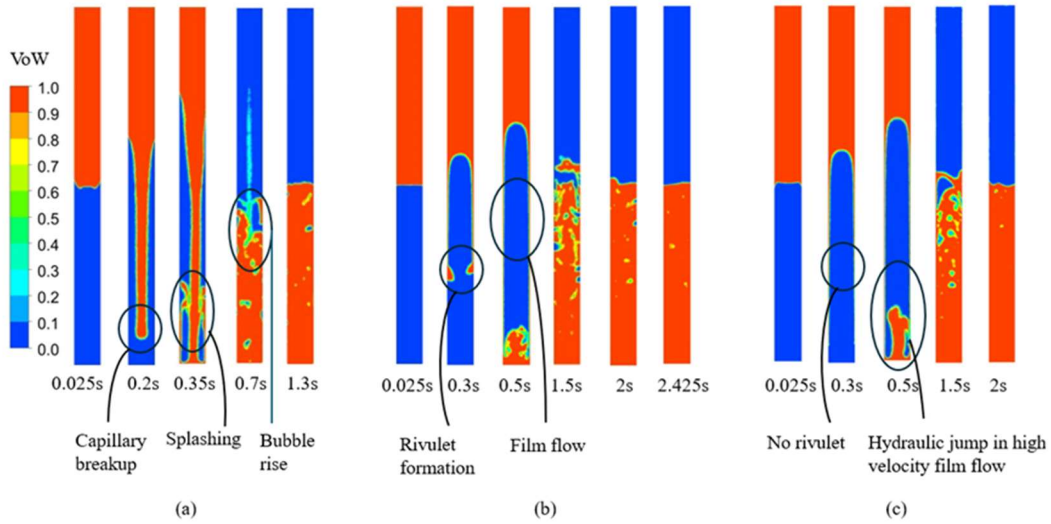

Figure 6. Water-volume fraction in the midplane for d= 100 mm and a) CA of 10 degrees, b) CA of 90 degrees, and C) CA of 170 degrees.

3.3. ROLE OF DIAMETER

Figure 7 demonstrates the effect of capillary diameter on dropdown time. We tested diameters of 3, 10 and 100 mm for different CAs. We observed that water was not dropping in most of the cases for superhydrophilic coatings, or CA of 10 degrees. For 3- and 10-mm (except 170-degree wettability wall) diameter channels, there were no flow. This implies that the viscous force was dominant, and the inertial force was too weak to break the stability of the air/water interface. The stable air/water interface was flat, as shown in Figure 8a for d = 3 mm, CA = 90 degrees. But it was curved downwards for d = 3 mm, CA = 170 degrees, as depicted in Figure 8b. This proved that superhydrophobic coatings had the lowest affinity for water, but it was still insufficient to break up the stability. From Figure 8c, we observed the interface was flat for d = 10 mm and a CA of 90 degrees. The first flow was observed at d = 10 mm, CA = 170 degrees. The flow dropped through the vessel wall, as shown in Figure 8d. As viscous force was still dominant, no splashing and lower air entrapment was observed. For large-diameter channels where inertia force is dominant, the liquid breaks up the stable interface by amplified perturbation over multiple positions, as seen in Figure 8e. The water dropped in contact with the wall, accompanied by free fall. This finger-like protrusion of the water column merged and dropped as a single column. This flow pattern generated swirl in counter directions, and the highest air entrapment was observed because of the oscillating interface. So, d = 100 mm had lower drop-down time because of inertia-force dominance than did d = 10 mm with CA of 170 degrees, which had a lower drop-down time than a CA of 90 degrees.

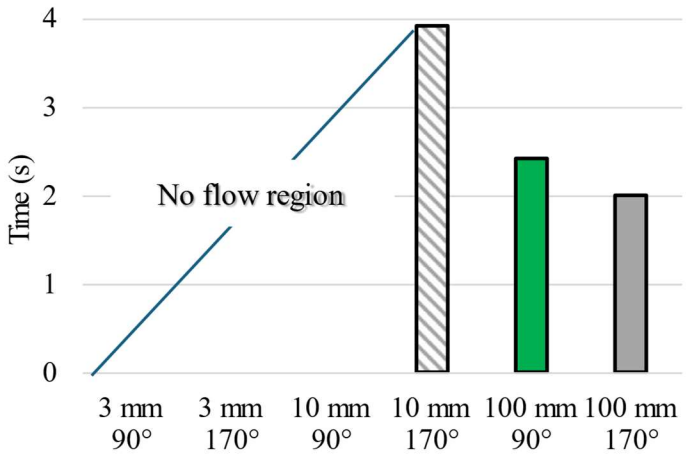

Figure 7. Effect of Channel diameter on dropdown for sealed vessel with different CA.

3.4. ROLE OF GRAVITY

In our experiment, we analyzed the impact of gravity on the drop-down time of water within a tube of 100 mm diameter and a CA of 90 and 170 degrees. The tests employed two different gravitational accelerations, 3.72 and 9.81 ms^{-2}, representing the gravitational forces of Mars and Earth, respectively. As depicted in Figure 9, the drop-down time for water was measured under different conditions. For a CA of 90 degrees in Earth's gravity, the drop-down time was 2.42 s whereas it was 2 s for a CA of 170 degrees. Conversely, under Martian gravity, the drop-down times were 3.88 s and 3.84 s for CAs of 90 and 170 degrees, respectively. Notably, the water-drop rate was faster for superhydrophobic walls (CA of 170 degrees) than for normal walls (CA of 90 degrees) in both gravitational environments. The drop time was higher in reduced gravity condition.

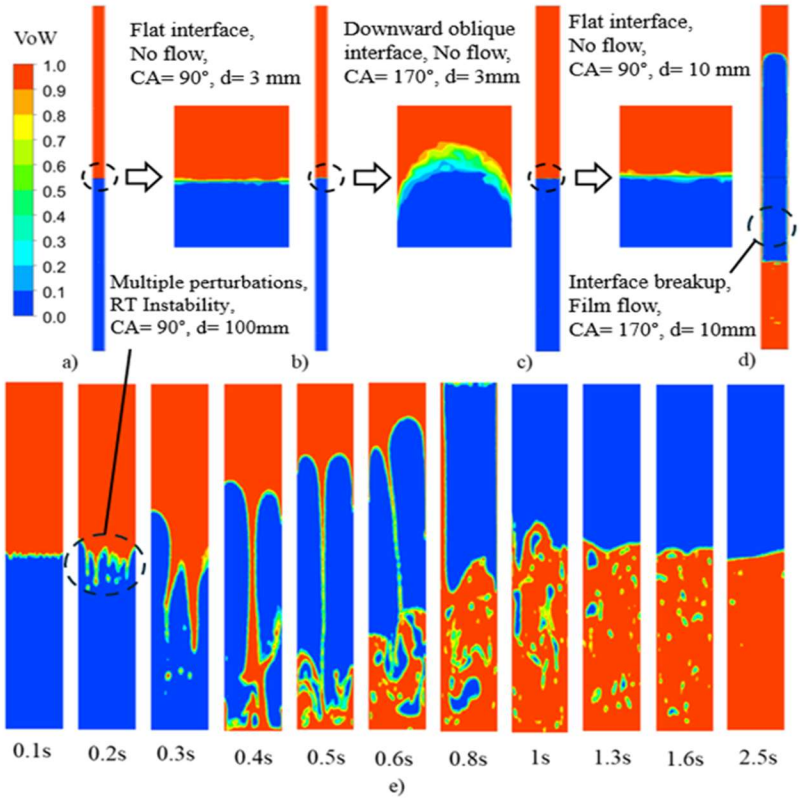

Figure 8. Water-volume fraction for different diameter channels a) d= 3 mm, CA= 90 degrees, b) d= 3 mm, CA= 170 degrees, c) d= 10 mm, CA= 90 degrees, d) d= 10 mm, CA= 170 degrees, and e) d= 100 mm, CA= 90 degrees.

This is attributed to the reduction in the gravitational and inertial forces at the lower gravitational acceleration of Mars, leading to a scenario where surface tension and viscous forces become more pronounced, thus affecting the Bo. The Bo decreased from 1358 to 515 for 90-degree wall when g changed from 9.78 to 3.72 ms^{-2}. Figure 10 showcases the flow patterns for CAs of 90 and 170 degrees under Martian gravity. The flow patterns observed were notably erratic and unstable in the low-gravity conditions. This unpredictable, unsteady flow pattern aligns with observations from previous studies that reported similar behavior in bounded capillaries under RT instability (Dinesh & Narayanan, 2021b). Such unpredictable flow patterns can have significant implications for

the reliability of systems like heat pipes that rely on the stability of fluid flow, especially in space applications where varying gravitational conditions are prevalent. This underscores the need for further research to gain a deeper understanding of the hydrodynamics and thermodynamics involved, and to develop strategies for mitigating the effects of low gravity on fluid flow and RT instability in critical systems.

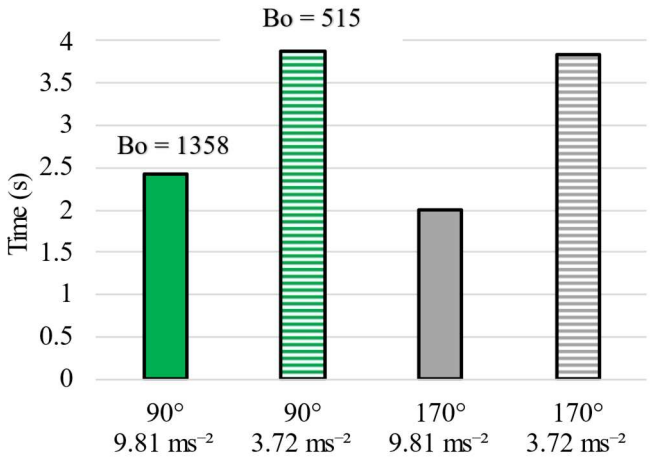

Figure 9. Gravity vs dropdown time for sealed vessel with different CA, and d = 100 mm.

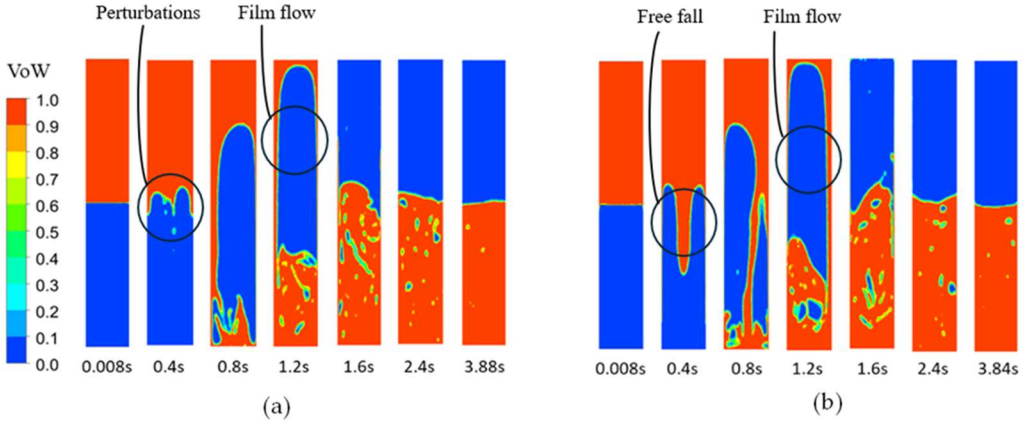

Figure 10. Gravity vs dropdown time at g = 3.72 ms^{-2}: d = 100 mm a) CA 90 degrees and b) CA = 170 degrees.

3.5. ROLE OF VISCOSITY

Heat pipes and chemical reactors employ a variety of working fluids, the selection of which depends on factors such as operating-temperature range, chemical stability, viscosity, thermal conductivity, and more (Faghri, 2012). Silicone oil shares many physicochemical properties with water, with viscosity being a notable exception. The viscosity of silicone oil is 19 times greater than that of water, making it an excellent candidate for examining the influence of viscosity on RT instability, with water serving as a point of comparison. Figure 11 presents the time it takes for the fluid to drop down to a CA of 170 degrees in vessels with dimensions d = 10 and 100 mm. It was observed that, for the same d and CA, the drop-down time was longer in channels filled with silicone oil compared to those filled with water. This indicates that an increase in viscosity extends the drop-down time. The Oh is higher for silicone oil than water signifying dominance of viscosity. The Oh is lower for 100 mm diameter vessels than 10mm ones indicating inertial dominance in large diameter channels further explain the faster dropdown time. Figure 12 depicts the flow patterns of water and silicone oil as they descend in sealed channels. In Figure 12a, the descent of water in a d = 10 mm channel occurred as thin film flow. In contrast, Figure 12b reveals the formation of rivulets on the vertical wall in the case of silicone oil flow. The elevated viscosity of silicone oil opposes the flow, causing the fluid to accumulate into rivulets. These rivulets eventually fall due to gravitational forces, resulting in a wavy pattern of the liquid film. It had the lowest amount of bubble entrapment.

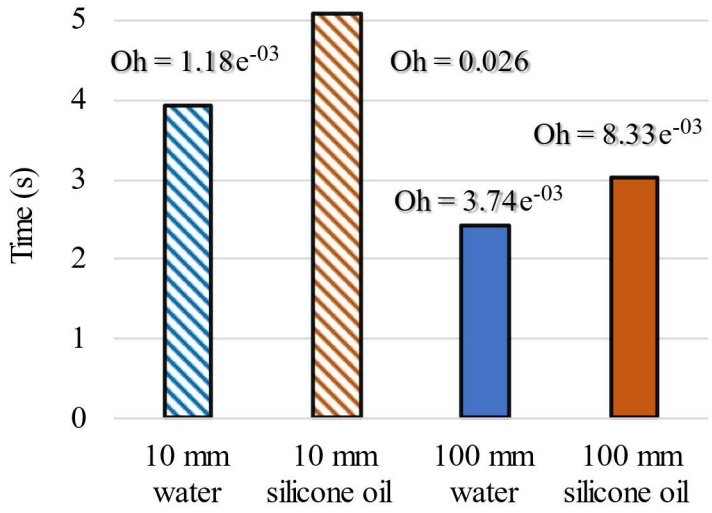

Figure 11. Viscosity vs dropdown time for sealed vessels with different diameter and CA = 170° walls.

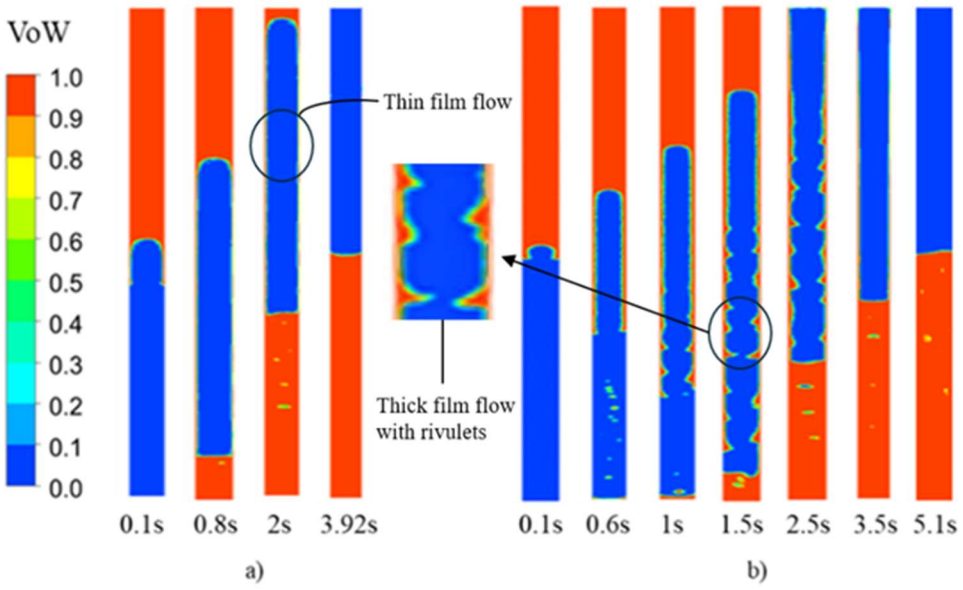

Figure 12. Effect of viscosity on flow pattern d = 10 mm and CA = 170 degrees with a) water and b) silicone oil.

4. CONCLUSIONS

Engineering applications, such as reactor system's ECCS water injection and gravitational heat pipes have water over top of air or steam in a closed channel. This configuration can produce flooding or concurrent flow-limiting water injection in LOCA in nuclear reactors. Higher liquid condensation in the condenser, even at an evaporator, can deteriorate heat-pipe performance though flow blockage, flow reversal, and flow instabilities. Therefore, in this study we checked flow behavior in terms of dropdown performance on an adiabatic domain and how CA, channel diameter, gravity, and viscosity can affect flow. We used the VOF method with sharp interface modeling to simulate the flow.

These are the following observations and remarks based on the simulation results:

- The VOF method with sharp interface modeling was employed to simulate the flow. It was observed that the overall static pressure in a sealed vessel exhibited a similar pattern across capillaries to tubes. As the RT instability in the closed system was found to produce lower dropdown velocity, the static pressure contour exhibited negligible local variation at any given moment.
- The effect of CA on flow blockage and RT-instability-induced dropdown was examined for 10, 50-, 90-, 130-, and 170-degree CAs. The results revealed that surfaces with higher wettability (i.e., CA <90 degrees) exhibited a strong affinity for water, leading to a breakdown in the initially stable air/water interface in the hanging portion, preventing water from dropping via the contact wall. This configuration resulted in the fastest dropdown due to free fall. The We is highest for superhydrophilic walls.

- Channel diameters of 3, 10, and 100 mm were analyzed to assess the effect of diameter on flow blockage. No flow was observed for a diameter of 3 mm due to higher viscous and surface tension force. Furthermore, no flow was observed for a 10-mm-diameter channel at CA of 10 and 90 degrees for the same reasons. For a contact angle of 170 degrees, water was observed to dropdown in 10-mm-diameter channels. Water dropped down via contact walls and middle portion by interface breakup for the 100-mm-diameter channels.
- The gravitational constant was varied to evaluate its effect on dropdown performance, with a higher dropdown time observed at lower gravitational values due to reduced inertial or gravitational dominance compared to viscous and surface-tension forces (lower Bo). The flow was also found to be unpredictable and unsteady under reduced gravity conditions.
- Two different fluids, water, and silicone oil were tested to examine the effect of viscosity. Silicone-oil flow was the slowest among all tests performed due to a high dominance of viscous forces (higher Oh), forming rivulets while dropping down via the contact wall. It exhibited the lowest turbulence during the dropdown.

ACKNOWLEDGEMENT

This work was supported in part by the Kummer Institute at Missouri University of Science and Technology through the Kummer Innovation and Entrepreneurship Doctoral Fellowship bestowed to the first author. The authors also extend their appreciation to the Missouri University of Science and Technology for granting access to high-performance computation and software.

REFERENCES

Angeli, P., & Gavriilidis, A. (2008). Hydrodynamics of Taylor flow in small channels: A review. *Proceedings of the Institution of Mechanical Engineers, Part C: Journal of Mechanical Engineering Science*, *222*(5), 737–751. https://doi.org/10.1243/09544062JMES776

Awati, V. B., Chavaraddi, K. B., & Gouder, P. M. (2019). Effect of boundary roughness on nonlinear saturation of Rayleigh-Taylor instability in couple-stress fluid. *Nonlinear Engineering*, *8*(1), 39–45. https://doi.org/10.1515/nleng-2018-0031

Brackbill, J. U., Kothe, D. B., & Zemach, C. (1992). A continuum method for modeling surface tension. *Journal of Computational Physics*, *100*(2), 335–354. https://doi.org/https://doi.org/10.1016/0021-9991(92)90240-Y

Dinesh, B., & Narayanan, R. (2021a). Branching behaviour of the Rayleigh-Taylor instability in linear viscoelastic fluids. *Journal of Fluid Mechanics*, *915*. https://doi.org/10.1017/jfm.2021.80

Dinesh, B., & Narayanan, R. (2021b). Branching behaviour of the Rayleigh-Taylor instability in linear viscoelastic fluids. *Journal of Fluid Mechanics*, *915*. https://doi.org/10.1017/jfm.2021.80

Eggers, J., & Villermaux, E. (2008). Physics of liquid jets. *Reports on Progress in Physics*, *71*(3). https://doi.org/10.1088/0034-4885/71/3/036601

Faghri, A. (2012). Review and advances in heat pipe science and technology. In *Journal of Heat Transfer* (Vol. 134, Issue 12). https://doi.org/10.1115/1.4007407

Gallaire, F., & Brun, P. T. (2017). Fluid dynamic instabilities: Theory & application to pattern forming in complex media. In *Philosophical Transactions of the Royal Society A: Mathematical, Physical and Engineering Sciences* (Vol. 375, Issue 2093). Royal Society. https://doi.org/10.1098/rsta.2016.0155

Grabaskas, D. (2019). *HEAT-PIPE MICROREACTORS*. https://www.nrc.gov/docs/ML1915/ML19150A609.pdf

Hassan, R. (2021). *Scholars' Mine Scholars' Mine Doctoral Dissertations Student Theses and Dissertations Dynamic behavior and interactions of ferrofluid droplets under Dynamic behavior and interactions of ferrofluid droplets under magnetic fields in low Reynolds number flows magnetic fields in low Reynolds number flows*. https://scholarsmine.mst.edu/doctoral_dissertations/3057

Höhne, T. (2022). CFD simulation of a heat pipe using the homogeneous model. *International Journal of Thermofluids*, *15*. https://doi.org/10.1016/j.ijft.2022.100163

Huhtamäki, T., Tian, X., Korhonen, J. T., & Ras, R. H. A. (2018). Surface Wetting Characterization using Contact Angle Measurements. *Nature Protocols*, 1521–1538. https://doi.org/10.1038/nprot.2018.032

Jose, J., & Kumar Hotta, T. (2023). A comprehensive review of heat pipe: Its types, incorporation techniques, methods of analysis and applications. In *Thermal Science and Engineering Progress* (Vol. 42). Elsevier Ltd. https://doi.org/10.1016/j.tsep.2023.101860

Khan, S. A., & Shah, A. (2019). Simulation of the two-dimensional Rayleigh-Taylor instability problem by using diffuse-interface model. *AIP Advances*, *9*(8). https://doi.org/10.1063/1.5100791

Khandekar, S., Panigrahi, P. K., Lefèvre, F., & Bonjour, J. (2010). LOCAL HYDRODYNAMICS OF FLOW IN A PULSATING HEAT PIPE: A REVIEW. *Frontiers in Heat Pipes*, *1*(2). https://doi.org/10.5098/fhp.v1.2.3003

Kundan, A., Nguyen, T. T. T., Plawsky, J. L., Wayner, P. C., Chao, D. F., & Sicker, R. J. (2017). Condensation on Highly Superheated Surfaces: Unstable Thin Films in a Wickless Heat Pipe. *Physical Review Letters*, *118*(9). https://doi.org/10.1103/PhysRevLett.118.094501

Kundan, A., Plawsky, J. L., Wayner, P. C., Chao, D. F., Sicker, R. J., Motil, B. J., Lorik, T., Chestney, L., Eustace, J., & Zoldak, J. (2015). Thermocapillary phenomena and performance limitations of a wickless heat pipe in microgravity. *Physical Review Letters*, *114*(14). https://doi.org/10.1103/PhysRevLett.114.146105

Leonard, B. P. (1979). A stable and accurate convective modelling procedure based on quadratic upstream interpolation. *Computer Methods in Applied Mechanics and Engineering*, *19*(1), 59–98. https://doi.org/10.1016/0045-7825(79)90034-3

Li, J., Wang, M., Fang, D., Wang, J., Liu, D., Tian, W., Qiu, S., & Su, G. H. (2021). CFD simulation on the transient process of coolant mixing phenomenon in reactor pressure vessel. *Annals of Nuclear Energy*, *153*. https://doi.org/10.1016/j.anucene.2020.108045

Liu, H., Vandu, C. O., & Krishna, R. (2005). Hydrodynamics of taylor flow in vertical capillaries: Flow regimes, bubble rise velocity, liquid slug length, and pressure drop. *Industrial and Engineering Chemistry Research*, *44*(14), 4884–4897. https://doi.org/10.1021/ie049307n

Maresz, K., Ciemięga, A., & Mrowiec-Białoń, J. (2020). Monolithic microreactors of different structure as an effective tool for in flow MPV reaction. *Chemical Engineering Journal*, *379*. https://doi.org/10.1016/j.cej.2019.122281

Menter, F. R. (1994). Two-equation eddy-viscosity turbulence models for engineering applications. *AIAA Journal*, *32*(8), 1598–1605. https://doi.org/10.1016/0029-554X(80)90461-9

Mucci, A., Kholi, F. K., Chetwynd-Chatwin, J., Ha, M. Y., & Min, J. K. (2021). Numerical investigation of flow instability and heat transfer characteristics inside pulsating heat pipes with different numbers of turns. *International Journal of Heat and Mass Transfer*, *169*. https://doi.org/10.1016/j.ijheatmasstransfer.2021.120934

Mulbah, C., Kang, C., Mao, N., Zhang, W., Shaikh, A. R., & Teng, S. (2022). A review of VOF methods for simulating bubble dynamics. *Progress in Nuclear Energy*, *154*, 104478. https://doi.org/https://doi.org/10.1016/j.pnucene.2022.104478

Murao, Y., Akimoto, H., Sudoh, T., & Okubo, T. (1982). Experimental study of system behavior during reflood phase of PWR-LOCA using CCTF. *Journal of Nuclear Science and Technology*, *19*(9), 705–719. https://doi.org/10.1080/18811248.1982.9734205

Oliveira, A. V. S., Stemmelen, D., Leclerc, S., Glantz, T., Labergue, A., Repetto, G., & Gradeck, M. (2020). Velocity field and flow redistribution in a ballooned 7×7 fuel bundle measured by magnetic resonance velocimetry. *Nuclear Engineering and Design*, *369*. https://doi.org/10.1016/j.nucengdes.2020.110828

Sosnowski, M., Krzywanski, J., & Gnatowska, R. (n.d.). *Polyhedral meshing as an innovative approach to computational domain discretization of a cyclone in a fluidized bed CLC unit*. https://doi.org/10.1051/4

Szymańska, K., Ciemięga, A., Maresz, K., Pudło, W., Malinowski, J., Mrowiec-Białoń, J., & Jarzębski, A. B. (2021). Catalytic Functionalized Structured Monolithic Micro-/Mesoreactors: Engineering, Properties, and Performance in Flow Synthesis: An Overview and Guidelines. *Frontiers in Chemical Engineering*, *3*. https://doi.org/10.3389/fceng.2021.789102

Tang, J., Zhang, F., Luo, X., & Zhai, Z. (2021). Effect of Atwood number on convergent Richtmyer–Meshkov instability. *Acta Mechanica Sinica*, *37*(3), 434–446. https://doi.org/10.1007/s10409-020-01015-5

Testoni, R., Bersano, A., & Segantin, S. (2021). Review of nuclear microreactors: Status, potentialities and challenges. In *Progress in Nuclear Energy* (Vol. 138). Elsevier Ltd. https://doi.org/10.1016/j.pnucene.2021.103822

Tusar, M. H., Bhowmik, P. K., Salam, B., Uddin Ahamed, J., & Kim, J. K. (2021). Convective heat transfer and friction factor characteristics of helical strip inserted annuli at turbulent flow. *International Journal of Heat and Mass Transfer*, *176*, 121422. https://doi.org/10.1016/j.ijheatmasstransfer.2021.121422

Ul Hassan, R., Lee, J., Khalil, S. M., Kang, G., Cho, D. H., & Byun, D. (2021). Experimental, Theoretical, and Numerical Investigation of the Electric Field and Surface Wettability Effects on the Penetration Length in Capillary Flow. *ACS Omega*, *6*(48), 32773–32782. https://doi.org/10.1021/acsomega.1c04629

Wang, D. Q., Yan, B. H., & Chen, J. Y. (2020). The opportunities and challenges of micro heat piped cooled reactor system with high efficiency energy conversion units. *Annals of Nuclear Energy*, *149*. https://doi.org/10.1016/j.anucene.2020.107808

Xu, W., Ouyang, K., Guo, J., He, H., He, X., & Liu, X. (2022). Experimental and numerical investigations on heat transfer and flow behavior of flow blockage in narrow rectangular channel with protrusions. *Applied Thermal Engineering*, *203*. https://doi.org/10.1016/j.applthermaleng.2021.117954

Youngs, D. (1982). *Time-Dependent Multi-material Flow with Large Fluid Distortion*. https://www.researchgate.net/publication/249970655

Youngs, D. L. (2013). The density ratio dependence of self-similar Rayleigh-Taylor mixing. In *Philosophical Transactions of the Royal Society A: Mathematical, Physical and Engineering Sciences* (Vol. 371, Issue 2003). Royal Society. https://doi.org/10.1098/rsta.2012.0173

Zanella, R., Tellier, R. Le, Plapp, M., Tegze, G., & Henry, H. (2021a). Three-dimensional numerical simulation of droplet formation by Rayleigh–Taylor instability in multiphase corium. *Nuclear Engineering and Design*, *379*. https://doi.org/10.1016/j.nucengdes.2021.111177

Zanella, R., Tellier, R. Le, Plapp, M., Tegze, G., & Henry, H. (2021b). Three-dimensional numerical simulation of droplet formation by Rayleigh–Taylor instability in multiphase corium. *Nuclear Engineering and Design*, *379*. https://doi.org/10.1016/j.nucengdes.2021.111177

SECTION

3. CONCLUSIONS AND RECOMMENDATIONS

In conclusion, this thesis has made advances in the understanding of thermal-hydraulic phenomena and flow behavior in sealed vessels in the context of nuclear reactor systems using Computational Fluid Dynamics (CFD) simulations. The analysis performed in the Replacement Research Reactor (RRR) and the Missouri University of Science and Technology Reactor (MSTR) have provided in-depth insights into the fluid flow and heat transfer processes that are critical to the design and operation of nuclear reactors.

The findings from the RRR model highlight the detailed flow characteristics and temperature profiles that can be expected at higher operational capacities. The study effectively demonstrated the utility of both realistic and porous media models, each serving unique purposes in the design and analysis of reactor safety systems. This knowledge contributes to a more robust framework for predicting performance under various operational scenarios, including potential design modifications or power uprates.

In exploring the complex dynamics of emergency core-cooling systems (ECCS) and gravitational heat pipes, the study on liquid drop down behavior illuminated the influence of multiple factors, such as contact angle, channel diameter, gravity, and fluid viscosity, on two-phase flow behavior. The use of the Volume-of-Fluid (VOF) method with sharp interface modeling provided a clear picture of how these variables affect the performance and reliability of ECCS and heat pipes, leading to potential improvements in emergency response capabilities.

The computational investigations undertaken in this thesis demonstrated the versatility and power of CFD as an important tool in the field of nuclear engineering. By offering a computationally efficient approach to complement experimental and theoretical studies, the research has bridged gaps between complex physical phenomena and practical application, ensuring that safety remains the paramount concern in the development and operation of nuclear reactors.

As the world continues to seek safe and sustainable energy solutions, the role of nuclear energy becomes increasingly prominent. The contributions of this thesis are timely and relevant, as they provide a scientific basis for the continued improvement of nuclear safety systems. Future research can build upon these findings to explore new designs, materials, and configurations that could further optimize reactor safety and efficiency. The goal moving forward is to harness the immense potential of nuclear energy while upholding the highest standards of safety and environmental stewardship.

BIBLIOGRAPHY

Bhowmik, P. K., Schlegel, J. P., & Revankar, S. (2022). State-of-the-art and review of condensation heat transfer for small modular reactor passive safety: Experimental studies. In International Journal of Heat and Mass Transfer (Vol. 192). Elsevier Ltd. https://doi.org/10.1016/j.ijheatmasstransfer.2022.122936

Kutbay, F., & Şentürk Lüle, S. (2023). The development of multi-physics approach with Monte Carlo and computational fluid dynamics coupling for reactor cores. Nuclear Engineering and Design, 402. https://doi.org/10.1016/j.nucengdes.2022.112127

Liao, J., Kucukboyaci, V. N., & Wright, R. F. (2016). Development of a LOCA safety analysis evaluation model for the Westinghouse Small Modular Reactor. Annals of Nuclear Energy, 98, 61–73. https://doi.org/10.1016/j.anucene.2016.07.023

Podila, K., Li, C., Azih, C., & Chen, Q. (2023). Modelling of heat transfer in a molten salt loop using computational fluid dynamics. Progress in Nuclear Energy, 164. https://doi.org/10.1016/j.pnucene.2023.104880

Song, J., An, W., Wu, Y., & Tian, W. (2018). Neutronics and thermal hydraulics analysis of a conceptual ultra-high temperature MHD cermet fuel core for nuclear electric propulsion. Frontiers in Energy Research, 6(APR). https://doi.org/10.3389/fenrg.2018.00029

VITA

Mehedi Hasan Tusar was born in Chittagong, Bangladesh. He completed his Bachelor of Science in Mechanical Engineering from Chittagong University of Engineering and Technology (CUET), graduating in January 2019. Following his undergraduate education, Mehedi has held the role of Executive in Engineering at NIRO JMI PHARMA LTD, managing operations and the implementation of a substantial upgrade project for the Effluent Treatment Plant. He also worked as research assistant at the Biomedical Device Lab in Seoul, South Korea, from September 2020 to September 2021. Immediately after he pursued further studies in the United States, where he earned his Master of Science in Nuclear Engineering from Missouri University of Science & Technology in May 2024. During his time at Missouri University of Science & Technology, Mehedi was a Kumner Innovation and Entrepreneurship Fellow, a position in which he evaluated thermal hydraulics of microreactor heat pipes and open pool type nucelar reactors using CFD techniques.